Department of Civil Engineering

Uncertainty management for the probabilistic simulation of the thermal resistance of fire barriers

Deepak Paudel

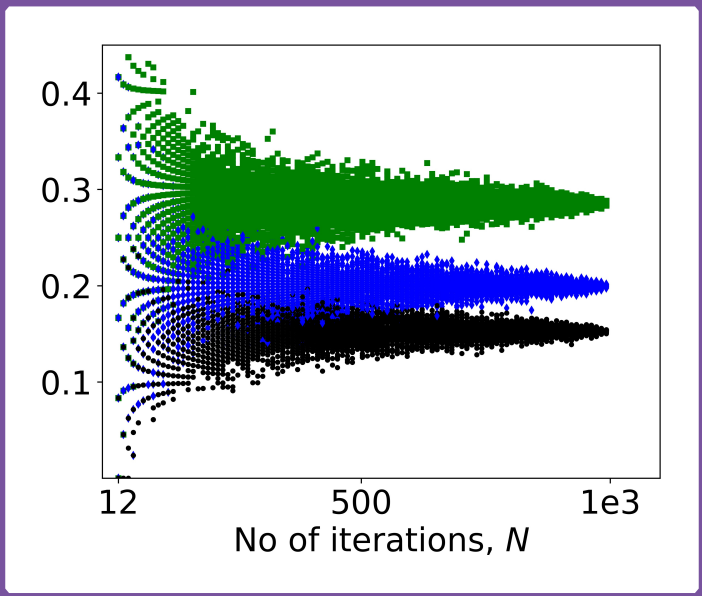

Aalto University

DOCTORAL DISSERTATIONS

Aalto University publication series
DOCTORAL DISSERTATIONS 186/2020

Uncertainty management for the probabilistic simulation of the thermal resistance of fire barriers

Deepak Paudel

A doctoral dissertation completed for the degree of Doctor of Science (Technology) to be defended, with the permission of the Aalto University School of Engineering, on 26 November 2020 at 12:00.

Aalto University
School of Engineering
Department of Civil Engineering
Civil Engineering (ENG030Z)

Supervising professor
Associate professor Simo Hostikka, Aalto University, Finland

Preliminary examiners
Assistant Professor Ruben Van Coile, Ghent University, Belgium
Dr David Lange, University of Queensland, Australia

Opponent
Assistant Professor Ruben Van Coile, Ghent University, Belgium

Aalto University publication series
DOCTORAL DISSERTATIONS 186/2020

ISBN 978-952-64-0135-5 (printed)
ISBN 978-952-64-0136-2 (pdf)
ISSN 1799-4934 (printed)
ISSN 1799-4942 (pdf)
http://urn.fi/URN:ISBN:978-952-64-0136-2

Unigrafia Oy
Helsinki 2020

Finland

Printed matter
4041-0619

Author
Deepak Paudel

Name of the doctoral dissertation
Uncertainty management for the probabilistic simulation of the thermal resistance of fire barriers

Publisher School of Engineering

Unit Department of Civil Engineering

Series Aalto University publication series DOCTORAL DISSERTATIONS 186/2020

Field of research Civil Engineering (ENG030Z)

Date of the defence 26 November 2020

Permission for public defence granted (date) 14 October 2020 **Language** English

☐ **Monograph** ☒ **Article dissertation** ☐ **Essay dissertation**

Abstract

Due to the inadequate availability of engineering tools, the conventional test-based method, currently, regulates the design of fire barriers. This thesis aims to provide a supporting simulation-based approach. The objective is to develop numerical models and a simulation framework for the prediction of fire barrier thermal resistance under uncertain fire load and material conditions. The main challenges are the complexity of the thermal behaviour of fibrous barriers to be simulated, the high computational cost of the stochastic simulations accounting for the input uncertainties, and the propagation of model uncertainty to the output distribution.

To predict the thermal behaviour of the stone wool, I present a multiphysics model of a fibrous layer, capable of tracking the heat transfer, chemical decomposition and oxygen transfer. As an alternative, I use heat conduction -based model with reaction kinetics coupled to the stone wool's organic content. The results show that the exothermic oxidation of the stone wool's organic matter is responsible for the observed peaks in the cold-side surface temperatures, but the amount of released energy and the height of these temperature peaks are limited by the unavailability of oxygen in stone wools with high organic content.

To reduce the computational burden of the probabilistic fire barrier resistance evaluation, I present the use of the Response Surface Method (RSM) and Gaussian Process (GP) regression. The results show that the simple polynomial-based RSM approximation fails when the heat transfer is affected by exothermic reactions. Fortunately, this is in contrast with GP, where the kernel combination made the approximation possible even for such a case.

Alongside, I studied the propagation of modelling uncertainty to the predicted output distributions using various examples: compartment fire experiment, stone wool thermal resistance test, a chain of two models, and meta-model based analysis. I propose a simple method of eliminating the propagated modelling uncertainty from the stochastically simulated output distribution. The results show that the proposed method effectively corrects the outputs if the uncertainty correction metric well represents the model uncertainty of the investigated stochastic analysis scenario. The illustrated examples mostly use normal or uniform input distributions, but the method is not bound to any distribution type.

Keywords fire barriers, uncertainty propagation, heat transfer

ISBN (printed) 978-952-64-0135-5	**ISBN (pdf)** 978-952-64-0136-2
ISSN (printed) 1799-4934	**ISSN (pdf)** 1799-4942
Location of publisher Helsinki	**Location of printing** Helsinki **Year** 2020
Pages 158	**urn** http://urn.fi/URN:ISBN:978-952-64-0136-2

Preface

During the final years of MSc studies, I showed career interest in numerical simulations, which lead me to MSc. thesis in heat transfer modelling. After that, I realized the need for uncertainty management in numerical modelling. On a similar topic, an opportunity was open for fire barriers, and it was a perfect time for me to begin this study.

I primarily thank Assoc. Prof. Simo Hostikka for this opportunity, and for agreeing to be the supervisor and advisor. Your supportive role and active project supervision were precious for the successful completion of the study. I thank my pre-examiners, Asst. Prof. Ruben Van Coile and Dr David Lange, for their valuable comments. I thank my co-authors, Aleksi Rinta-Paavola and Hannu-Petteri Mattila, for their contribution to my publication, and the preliminary studies of stone wool modelling. I thank my work colleagues, Hadi Bordbar, Kaiyuan Li, Rahul Kallada Janardhan and Teemu Isojärvi, it was great to be in this team. I thank, Topi Sikanen, a project co-member from VTT, and I thank my friends, Roman and Saani, for making this journey joyful.

Finally, I acknowledge the State Nuclear Waste Management Fund of Finland in the scope of the SAFIR-programs, the Finnish Fire Protection Fund (Palosuojelurahasto), Rakennustuotteiden laatu-säätiö, Nordic Nuclear Safety Research (NKS), and Paroc Oy for funding this work.

Deepak Paudel, Helsinki, November 3, 2020,

List of Publications

This thesis is based on the following publications. The publications are reproduced with permission from the publishers.

I. Paudel, D. and Hostikka, S., 2019. Propagation of modelling uncertainty in stochastic heat-transfer simulation using a chain of deterministic models. *International Journal for Uncertainty Quantification*, 9(1), pp.1-14. https://doi.org/10.1615/Int.J.UncertaintyQuantification.2018027275

II. Paudel, D. and Hostikka, S., 2019. Propagation of model uncertainty in the stochastic simulations of a compartment fire. *Fire Technology*, 55(6), pp.2027-2054. https://doi.org/10.1007/s10694-019-00841-9

III. Paudel, D., Rinta-Paavola, A., Mattila, HP., and Hostikka, S., 2020. Multiphysics modelling of stone wool fire resistance. *Fire Technology*, pp.1-30. https://doi.org/10.1007/s10694-020-01050-5

IV. Paudel, D., and Hostikka, S., 2020. Meta-model based stochastic simulation of fire barrier cold-side temperature. *Fire Safety Journal*, pp.1-12. https://doi.org/10.1016/j.firesaf.2020.103175

Authors Contributions

Publication I: "Propagation of modelling uncertainty in stochastic heat-transfer simulation using a chain of deterministic models"

The author wrote the article, derived an uncertainty propagation model, carried out stochastic analysis using a chain of numerical models, and illustrated the uncertainty compensation technique. Co-author supervised and advised the work, developed study concepts and ideas, and commented on the article.

Publication II: "Propagation of model uncertainty in the stochastic simulations of a compartment fire"

The author wrote the article, constructed compartment fire models, further developed the uncertainty propagation model and validated both models using experimental data. Co-author supervised and advised the work, developed study concepts and ideas, and commented on the article.

Publication III: "Multiphysics modelling of stone wool fire resistance"

Aleksi Rinta-Paavola and Hannu-Petteri Mattila were responsible for conducting experiments and developing the preliminary material and heat transfer models. The author wrote the article, constructed the multiphysics model, further developed the heat-conduction model, and carried out sensitivity analysis using the models. Hostikka, S., supervised and advised the work, developed study concepts and ideas, and commented on the article.

Publication IV: "Meta-model based stochastic simulation of

fire barrier cold-side temperature"

The author wrote the article, developed Multinomial matrix method for RSM, constructed RSM and GP based meta-models for stochastic stone-wool thermal resistance problem, and demonstrated the meta-model uncertainty quantification and compensation method. Co-author supervised and advised the work, developed study concepts and ideas, and commented on the article.

Contents

Symbols

A	pre-exponential factor
c	heat capacity or constant term
d_f	fibre diameter
D	mass diffusion coefficient
D_2	surface diffusion coefficient
E_a	activation energy
e	emissivity
$\mathcal{GP}$	Gaussian process
Δh	enthalpy of combustion
h	heat transfer coefficient
k	conductivity or kernel function
K	covariance
l	stone wool thickness
n	reaction order or no of parameters
m	mean function or polynomial order
M	number of test or training points
Mn	multinomial matrix
N	sample size
Nt	time points
$\mathcal{N}$	normal distribution
P	probability
T	temperature
T_h	hot-side temperature
T_∞	ambient temperature

Greek Letters

θ	fibre mean angle
β	extinction coefficient or power term
δ	systematic bias
ϵ	error
ρ	density
σ	Stephan−Boltzmann constant
σ	standard deviation
ϕ	porosity
$\dot{\omega}$	reaction rate
μ	mean

Subscripts and superscripts

0	initial value
1	hot-side surface
2	cold-side surface
a	air
f	fibre
ij	indexes
o	organic content
p	product
s	solid
xx,s	specific density
$\hat{x}x$	observed quantity
Ln	linear
RQ	rational quadratic
SE	square exponential

1. Introduction

1.1 Background and motivation

Fire barriers are physical systems designed to delay the spreading of fire and smoke. In buildings, the examples of fire barrier are fire-rated doors and walls [1]. In industrial facilities, a fire barrier can also serve other purposes than the compartmentation. An example is the defence-in-depth concrete layers around a nuclear reactor for the prevention of the release of radioactive substance [2]. In other situations, a fire barrier can be a local protective layer between a likely fire source and the target to be protected [3].

Fire accidents in the early part of the 20^{th} century resulted in an excessive loss of life and property, which lead the development of fire safety building codes. The safety codes primarily regulate the design of barriers, based on the standard test carried out according to Annexe EN 1363-1 [4]. The design criteria are the insulation, integrity and load-carrying capacity. In other words, the barrier should prevent ignition on the unexposed side, spreading of smoke/fire to another compartment and structural failure during the time of event [5]. The test procedure consists of measuring the cold-side temperature of the sample exposed to a combustion chamber depicting ISO-834 standard fire [6]. The thermal actions predicted from such test, however, may not always correspond to the structural behaviour in the real fire event [7, 8].

The concept of simulation-based methods existed in the past, and over the period of last few decades the computing resources and simulation tools for fire safety engineering evolved significantly [9, 10, 11, 12, 13,

14, 15, 16, 17, 18, 39], which supported in enabling the simulation-based approach as a reliable means of evaluating the fire barrier performance [19, 20]. In practice, however, the safety measures are still dominated by the test-based approach because of the limited number of peer-reviewed case studies, lack of methods for the management of the prediction uncertainties, and lack of clarity on the position of probabilistic methods [21, 22, 23].

This study concentrates on the fulfilment of one of the design criteria and demonstrates the simulation-based approach of evaluating fire barrier thermal resistance. The focused design criterion is that the barrier should prevent ignition on the unexposed side. I elaborate on the challenges faced for such simulations using the following captions:

I. **Barrier thermal resistance**

The commonly used barrier materials are steel, concrete, gypsum, and stone-wool. Homogeneous structures like steel and concrete's thermal and material properties are already well established, and the response of such materials is straightforwardly solved using numerical methods such as the Finite Element Method (FEM) [25, 26]. For a porous structure such as gypsum and stone-wools, however, the heat transfer occurs in all three modes: conduction, convection and radiation, and the structure contains reactive material that decomposes at high temperature and triggers mass transfer within the structure [27, 28]. Furthermore, the availability of oxygen within the porous region affects the rate of the chemical reactions and the overall heating behaviour of the structure [1, 29]. The research question is:

How to predict the high-temperature heating behaviour of fibrous structure such as stone-wool?

II. **Probabilistic simulation**

The barrier thermal resistance evaluation is not merely a deterministic problem, due to the uncertainties associated with the fire conditions and barrier material properties, which vary between production batches and, especially, between different products and brands [30, 31, 32, 33]. The uncertainties are handled through sensitivity studies [35, 34], the use of safety factors such as Best Estimate Plus

Uncertainty (BEPU) [36] or probabilistic analysis [30]. The former two methods have been found practical for qualitative study and the known uncertainty types [37, 38, 39]. This work aims at quantitative evaluations of fire barrier resistance, for which the most reliable method is the probabilistic analysis [30]. The probabilistic analysis furthermore needs to be stochastic because the evaluation function is an iterative numerical procedure such as FEM, for which, an explicit derivation of the probabilistic outputs is not possible [40, 41]. The surrogate models or the meta-models are simplified and approximate functional representations of the actual deterministic models, commonly used to ease the computational burden stochastic simulations [42, 43, 44]. The previous works lack the study of the applicability of the meta-modelling techniques for barrier thermal resistance evaluation. The research question is:

What are the popular meta-modelling methods applicable to the barrier thermal resistance evaluation?

III. **Uncertainty propagation**

The modelling uncertainty is the measure of quantity by which the predicted output differs from the experimentally measured value. In fire safety engineering, the common practice is to compare the experiments with model simulations and to quantify the model uncertainties using two components, i.e., systematic bias, δ, and the relative second central moments of random errors, $\widetilde{\sigma}_{\epsilon}$ [45, 46]. The former one is the measure of average prediction shift from the measured value, and the latter one is the standard deviation of the random errors between the predicted and measured values. In a single deterministic analysis, δ and σ_{ϵ} are sufficient to postulate the prediction uncertainty [45]. In probabilistic simulations, the output is not a single value but distribution, and one cannot know in advance how the model uncertainty propagates [47, 48]. The methods necessary for the management of such uncertainty propagation are lacking [41]. Also, the use of meta-models means additional uncertainty, i.e., one may obtain the converged solution using meta-models but not necessarily the same as the one that corresponds to the actual deterministic model. Studies presenting the use of meta-models provide

the information of likelihood fraction by which the meta-model and actual model prediction differ [49, 50, 51, 52, 53, 54, 55, 56]. Nevertheless, such information is not sufficient to explain the discrepancy in terms of output distribution essential for accurate probabilistic prediction. The research question is:

How to quantify and compensate the model uncertainty in the probabilistic simulations?

1.2 Objective and scope of the thesis

This study supports the simulation-based alternatives to fire barrier design. The objective is to develop an application framework which functions as a roadmap for the probabilistic simulation of fire barrier resistance under uncertain fire and material conditions. I elaborate on it using the following distinguished captions reflecting the research questions raised in the earlier section.

I. **Modelling fibrous barrier thermal resistance**

There have been several attempts to model the heat transfer of a fibrous structure. Lee [57] investigated the effect of fibre orientation on the intra-fibre radiative heat transfer. Andersen and Dyrboel [58] predicted the radiative fluxes using Planck mean properties and compared them to the one obtained using spectral and flux-weighted properties. Veiseh and Hakkaki-Fard [59] estimated the thermal conductivity by numerically solving the steady-state radiative and conductive heat transfer, and compared it to the experimentally measured values. Some studies included the effect of organic material degradation on the overall heat transfer and suggested that the accurate prediction of stone wool heating behaviour would require the modelling of oxygen controlled decomposition reactions [60, 29, 1].

The objective is to develop a multiphysics model capable of solving both heat and mass transfer such that the oxygen controlled degradation rate would be applicable for the accurate prediction of stone wool heating behaviour. The models will be validated using the ex-

perimental data, and in comparison to classical heat conduction - based model with optimized decomposition kinetics.

II. **Probabilistic simulation using meta-model**

Two commonly used meta-modelling methods that have also found applications in fire safety engineering are Gaussian Processes (GP) Regression or Kriging and Response Surface Method (RSM). The GP Regression is a non-parametric approach of training a selected kernel function over the known input and output data, and optimizing the coefficients using the Bayesian inference [61, 62, 63]. This method has become popular in the field of machine learning, and there exist various open software platforms for GP modelling [64, 65, 66, 67]. On the other hand, the RSM is a simple statistical approach of expressing a scalar surface using the polynomials of inputs, and obtaining the coefficients of the polynomials by satisfying the surface with deterministic values [68, 69]. The method was first introduced in 1951 to determine the optimal conditions in the chemical investigation, it later evolved for time-variant non-linear problems, and recently it is also used for the approximation of FEM solutions [70, 71, 49, 72, 73]

The objective is to test both RSM and GP methods for the probabilistic analysis of barrier thermal resistance. As a random input, I will use a range of time-temperature curves representing various compartment fire scenarios.

III. **Uncertainty management**

There are various deterministic or stochastic methods to study uncertainty propagation [38]. In the former type, output uncertainty, as a function of input uncertainty, is the expression of Taylor chains, Hermite polynomials or basis functions [74, 75]. It is popular for linear problems with a relatively small range of uncertainties. Some examples are the generalized Polynomial Chaos (gPC), Gaussian closure, and Equivalent linearization [76, 77]. In the latter type, the limit state function runs for several iterations. The method is suitable when the derivatives of the limit state function are unworkable. Some examples are Monte-Carlo (MC), Latin Hypercube Sampling (LHS) and Fourier Amplitude Sensitivity Test (FAST) [78, 79, 37].

The objective is to study the propagation of model uncertainty for barrier thermal resistance problem, using the MC simulation, and to develop a methodology for the quantification and compensation of the propagated uncertainty. The methodology will be tested and validated for various barrier thermal resistance modelling scenarios.

2. Methods

In this chapter, I review the methods used in the present work. Section 2.1 presents stone wool fire resistance test, Finite Element Method (FEM) solution of the 1D parabolic diffusion equation, and FEM based multiphysics model and Fire Dynamics Simulator (FDS) heat conduction model simulating the fire resistance test. Section 2.2 presents a statistical method that I developed to quantify and compensate for the modelling uncertainty of stochastic simulations. Section 2.3 presents the stochastic analysis scenario for stone wool fire resistance test, and cost-efficient methods (RSM, GP) applied for the stochastic simulation.

2.1 Barrier thermal resistance

2.1.1 Thermal resistance test

The fire resistance test was carried out by Paroc Oy (now Owens Corning, Finland) [80]. Figure 2.1 shows the test set up, in which, a sample of size 60×60 cm having thickness l is separated from the combustion chamber using 1 mm thin metal sheet. The combustion chamber temperature, T_h, follows the ISO 834 standard fire curve, and the initial cold-side temperature is equal to that of ambient, T_∞,

$$T_{\mathrm{h}}(t) = T_\infty + 345\log_{10}(8t+1). \tag{2.1}$$

Altogether, 30 tests were performed with varying wool density, thickness and organic content. Table 2.1 lists the material and geometrical

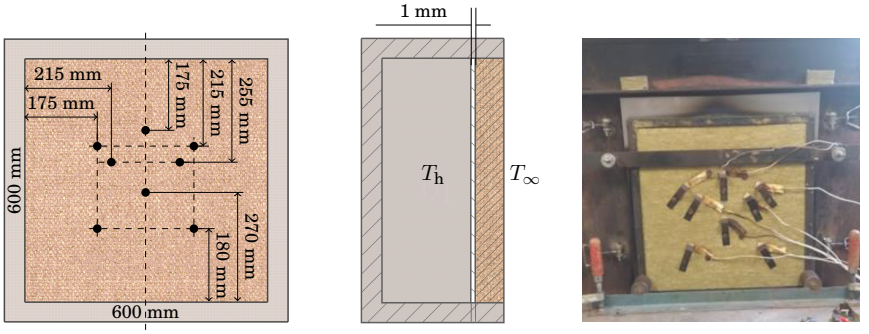

Figure 2.1. Test geometry for small scale fire resistance test, EN 1363-1. a) Sample size and thermocouple locations, b) Cross-section, c) Cold-side temperature measurements.

properties of the investigated stone wool types.

Table 2.1. Material and geometrical properties of the investigated stone wools.

Wool No.	Insulation thickness, l(mm)	Wool density, ρ_w(kgm^{-3})	Loss On Ignition (LOI) (%)	Intact fibre(%)	Fibre mean thickness, d_f (μm)	Fibre mean angle, θ (°)	Extinction coefficient, $\beta(m^{-1})$
1	61.9	101.4	1.5	63.2	4.7	3.6	2866
2	62.4	100.5	1.3	61.8	5.1	14.8	2620
3	60	97.2	1.4	60.1	4.6	19.3	2492
4	63.2	95.3	1.2	59.2	4.4	41.7	1936
5	61.7	100.7	1.2	61.1	4.6	46.4	1921
6	60.5	100.2	1.1	57.5	4.9	17.2	2441
7	60	99.6	1.1	62	3.7	29.9	2598
8	61.8	90.2	1.3	66.5	3.3	6.5	2979
9	61.1	69.8	1.3	62.2	3.3	6.5	2156
10	61.7	79.3	1.5	61.4	3.4	6.5	2394
11	60.1	90.3	1.3	56.1	4	4.9	2389
12	60.1	90.3	1.4	61.5	3.9	4.2	2639
13	61.4	100	1.4	62	4.4	4.3	2836
14	60.3	100.9	1.5	61.3	3.7	5.1	2978
15	61	138.8	2.1	64.6	3.8	1.5	4274
16	41.2	107.2	1.3	63.7	3.8	3	3278
17	72.7	78.9	1.6	65.7	3.3	6.5	2566
18	61.3	141.2	1.9	59.7	3.4	1.3	4154
19	61.9	147.7	1.5	59	5.3	1.9	3739
20	52	38.3	0.7	62.2	4.7	0.8	1076
21	60.5	147.3	1.3	56.4	3.2	1.5	4184
22	75.7	66.3	6.9	61.5	4	2.4	1819
23	75.2	71.1	9	62	4.1	1.9	1908
24	76.2	51.4	9.8	64.7	4.4	1	1395
25	71.5	63.9	1.1	58.1	4.3	2.9	1719
26	72.8	75.1	1.2	57.5	4.6	2.9	1953
27	60.4	85	1.3	61.5	4	3.8	2469
28	75	68.5	4.7	61.1	4.3	1.1	1869
29	75.7	48.7	6.7	61.6	4	1.5	1341
30	75.3	48.2	4.8	63.1	4.5	3.95	1334

The cold side surface temperatures were recorded using several K-type thermocouples. The right figure shows the installation of thermocouples. The installation complies with the European standard, EN 1363-1.

2.1.2 Finite element model

The temperature along the thickness, x, of barrier is solved using one-dimensional parabolic heat diffusion equation,

$$\rho c \frac{\partial T}{\partial t} = \frac{\partial}{\partial x}\left(k \frac{\partial T}{\partial x}\right). \tag{2.2}$$

The boundary conditions of Eq. 2.2 consist of a linear convective and a non-linear radiative heat-fluxes,

$$-k\frac{\partial T}{\partial x}\bigg|_{x=0} = -h_1(T_{\mathrm{h}} - T_1) - e\sigma(T_{\mathrm{h}}^4 - T_1^4), \tag{2.3}$$

$$-k\frac{\partial T}{\partial x}\bigg|_{x=l} = -h_2(T_2 - T_\infty) - e\sigma(T_2^4 - T_\infty^4). \tag{2.4}$$

A FEM solution to a discrete system, Figure 2.2, using 1^{st} order shape

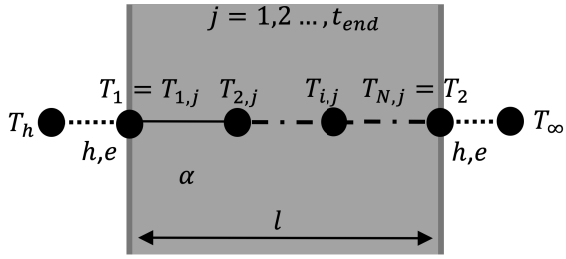

Figure 2.2. One dimensional finite discretization of the heat diffusion domain. α represents the wall material parameters.

function and explicit Euler time scheme is [81]

$$\mathbf{T}_{1..N,t} = [\mathbf{C}]^{-1}\left[(\mathbf{C} - \Delta t\mathbf{K})\mathbf{T}_{1..N,t-1} - \Delta t\mathbf{F}\right], \tag{2.5}$$

where $\mathbf{K}$, $\mathbf{C}$ and $\mathbf{F}$ are conductance matrix, capacitance matrix and force vector given as

$$\frac{k}{\Delta l}\begin{pmatrix} 1 & -1 & \cdots & 0 & 0 \\ -1 & 2 & \cdots & 0 & 0 \\ \vdots & \vdots & \ddots & \vdots & \vdots \\ 0 & 0 & \cdots & 2 & -1 \\ 0 & 0 & \cdots & -1 & 1 \end{pmatrix}, \frac{\rho c_p \Delta l}{6}\begin{pmatrix} 2 & 1 & \cdots & 0 & 0 \\ 1 & 4 & \cdots & 0 & 0 \\ \vdots & \vdots & \ddots & \vdots & \vdots \\ 0 & 0 & \cdots & 4 & 1 \\ 0 & 0 & \cdots & 1 & 2 \end{pmatrix}, \text{ and } \begin{pmatrix} F_{1,t} \\ 0 \\ \vdots \\ 0 \\ F_{2,t} \end{pmatrix}$$

respectively, where $F_{1,t} = -h(T_{\mathrm{g}} - T_{1,t-\Delta t}) - e\sigma(T_{\mathrm{g}}^4 - T_{1,t-\Delta t}^4)$ and $F_{2,t} = -h(T_{N,t-\Delta t} - T_\infty) - e\sigma(T_{N,t-\Delta t}^4 - T_\infty^4)$.

2.1.3 Stone wool model: Multiphysics

In this section, I present the main features of the multiphysics model. The details are provided in [82].

The stone wool with density ρ_{w} consists of fibres (ρ_{f}), organic material (ρ_{o}), products of the decomposed organic matter (ρ_{p}), and air (ρ_{a}),

$$\rho_{\mathrm{w}} = \rho_{\mathrm{f}} + \rho_{\mathrm{o}} + \rho_{\mathrm{a}} + \rho_{\mathrm{p}}. \tag{2.6}$$

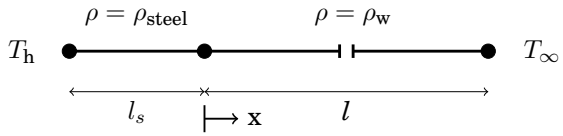

Figure 2.3. Multiphysics model computational set up. l_s and l are the steel plate and stone wool thicknesses, respectively. The gap in the stone wool indicates that the lengths are not in scale ($l >> l_s$).

The mass transfer in the stone wool domain triggers due to the decomposition of the organic matter [28]. As the information of the exact chemical composition and reaction steps are not available, I assume an approximate single step scheme consisting of two lumped gas species, air and products,

$$\mathrm{C_8H_6O_2} + 5.5(\overbrace{\mathrm{O_2} + 3.76\mathrm{N_2}}^{\text{Air}}) \rightarrow \overbrace{5\mathrm{CO_2} + 20.7\mathrm{N_2} + 3\mathrm{H_2O}}^{\text{Products}} + 3\mathrm{C}, \tag{2.7}$$

where, 1g of organic matter when reacts with 5.63g of air produces 6.45g gas products and 0.27g char.

The mass transfer is assumed to be purely diffusive. The solved governing equations and their initial conditions are the continuity equation for organic mass, diffusion equation for the products mass, and the diffusion equation for the enthalpy in the slab:

$$\frac{\partial \rho_{\mathrm{o}}}{\partial t} = -\dot{\omega}\rho_{\mathrm{w}}, \qquad 0 \leq x \leq l, \qquad \rho_{\mathrm{o},0} = \mathrm{LOI} \cdot \rho_{\mathrm{w}}, \tag{2.8}$$

$$\frac{\partial \rho_{\mathrm{p}}}{\partial t} = \frac{\partial}{\partial x}\left(D\frac{\partial \rho_{\mathrm{p}}}{\partial x}\right) + \dot{\omega}\rho_{\mathrm{w}} f, \qquad 0 \leq x \leq l, \qquad \rho_{\mathrm{p},0} = 0, \tag{2.9}$$

$$\rho c \frac{\partial T}{\partial t} = \frac{\partial}{\partial x}\left(k \frac{\partial T}{\partial x}\right) + \dot{\omega}\rho_{\mathrm{w}}\Delta h, \qquad -l_s \leq x \leq l, \qquad T_0 = T_\infty. \tag{2.10}$$

The factor ($f = 6.45$) is according to the decomposition scheme Eq. 2.7. The organic matter heat of combustion (Δh) is 25 MJkg^{-1}. The rate of the oxidation reaction, $\dot{\omega}$, is assumed to follow an Arrhenius form

$$\dot{\omega} = A e^{\left(-\frac{E_{\mathrm{a}}}{\mathrm{R}T}\right)} \left(\frac{\rho_{\mathrm{o}}}{\rho_{\mathrm{w}}}\right)^{n} X_{\mathrm{O_2}}^{n_{\mathrm{O_2}}}. \tag{2.11}$$

Here, $X_{\mathrm{O_2}}$ is the oxygen volume fraction calculated using the volume proportions of the air and products,

$$X_{\mathrm{O_2}} = 0.21 X_{\mathrm{a}}, \quad X_{\mathrm{a}} = 1 - X_{\mathrm{p}}, \quad X_{\mathrm{p}} = \frac{\rho_{\mathrm{p}}\rho_{\mathrm{a,s}}}{\rho_{\mathrm{p,s}}}, \tag{2.12}$$

where 0.21 is the oxygen volume fraction in air.

Regarding the boundary conditions, I assume that the gas diffusion is blocked on the hot-side, depends upon the surface diffusion coefficient (D_2) on the cold side, and the radiative and convective heat fluxes affect on both sides.

The stone wool bulk properties depend on T or ρ_{o}, or both, and are calculated by assuming the medium between the fibres to be air. The bulk heat capacity is the weighted fraction of fibre, organic matter, and air. The bulk thermal conductivity is according to Karamanos approach [60], in which, the equivalent expression includes conductive and radiative part. The conductive part includes the parallel and the perpendicular components that depend upon porosity (ϕ). The radiative part is calculated using the refractive index value $n = 1.2$, Stephan-Boltzmann constant (σ), and extinction coefficient (β).

The heat transfer coefficient on the hot-side is $h_1 = 18.5$ Wm^{-2}K^{-1}, and on the cold-side (h_2), it is qualitatively close to the natural convection of a vertical wall. The gas diffusivity (D) is calculated using Chapman and Enskog equation [83]. The gas diffusion coefficient on the cold-side (D_2) is assumed to be 10^{-3} order of h_2.

The chemical decomposition parameters (A, E_{a}, n and $n_{\mathrm{o_2}}$) are optimized by finding a minimum error in the cold-side temperatures. For this, a Monte-Carlo (MC) simulation was carried out using the sample range listed in Table 2.2. The search criterion is the mean square error, the

sampling method is Latin Hypercube Sampling (LHS), and the sample size is 1000. The fifth column shows the optimized values.

Table 2.2. The sample spaces and the optimum values for the chemical decomposition parameters.

Parameters	Distribution	Lower	Upper	Optimum	Unit
Frequency factor, A	Uniform	5.0E2	1.5E3	1.07E3	s^{-1}
Activation energy, E	Uniform	5.0E4	1.5E5	9.30E4	$Jmol^{-1}$
Reaction order, n	Uniform	0.4	1.0	0.7	-
Reaction order, n_{o_2}	Uniform	0.4	0.8	0.6	-

The numerical implementation is using the Finite Element Method (FEM) and a custom Python script. The finite elements are linear and uniform of size 1 mm. The time discretization follows the explicit Euler method. The time step size is adaptive to the maximum temperature rise of 1 °C. The solver adopts a size between a millisecond to about a hundred seconds.

The numerical convergence was tested by comparing the results with reduced element size (0.5 mm). The maximum change in the cold-side temperature was less than 0.3%. The predictions were also benchmarked using COMSOL Multiphysics. The maximum difference in temperature prediction was $\simeq 3\%$.

2.1.4 Stone wool model: Heat conduction

A separate model was constructed using the one-dimensional heat conduction model of Fire Dynamics Simulator (FDS), a commonly used tool for fire-driven flows and pyrolysis of structures [10]. The model solves parabolic heat diffusion equation coupled to the Arrhenius equation,

$$\rho c \frac{\partial T(x,t)}{\partial t} = \frac{\partial}{\partial x}\left(k \frac{\partial T(x,t)}{\partial x}\right) + \dot{\omega}\rho_{\mathrm{w}}\Delta h, \quad \dot{\omega} = \mathrm{A}e^{\left(-\frac{\mathrm{E_a}}{\mathrm{RT}}\right)}\left(\frac{\rho_{\mathrm{o}}}{\rho_{\mathrm{w}}}\right)^n. \quad (2.13)$$

The stone wool bulk properties are defined to change only to temperature. The chemical decomposition parameters are optimized concerning the organic material mass %.

Figure 2.4 shows the optimization steps. First, MC simulations were carried out for N=1000 samples of A, E_{a} and n, generated using the LHS technique and the range listed in Table 2.2. Then, comparing the least square error in the cold-side temperatures, the optimal A, E_{a} and n val-

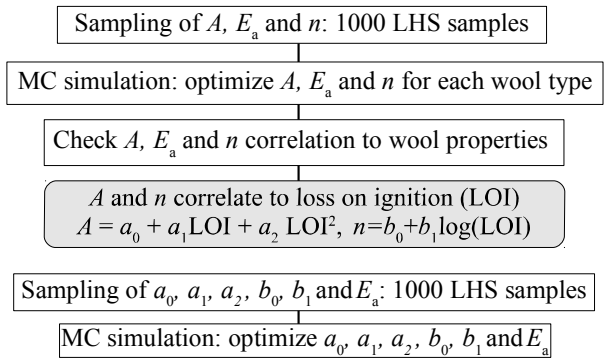

Figure 2.4. Steps for the optimization of the chemical decomposition parameters: A, E_a and n.

ues were selected for each wool types. The optimized values were plotted against LOI, density and thickness. The values did not correlate with density or thickness. Similarly, the E_a did not correlate with any of the properties. A and n, however, did correlate to LOI as the second-order polynomial and logarithmic expansion,

$$A = a_0 + a_1 \mathrm{LOI} + a_2 \mathrm{LOI}^2, \quad \text{and} \quad n = b_0 + b_1 \log(\mathrm{LOI}), \tag{2.14}$$

respectively. Then the second round MC simulation was carried out to optimize the coefficients, a_0, a_1, a_2, b_0, b_1, and E_a.

The correlations are based on the independently optimized values of the different types of stone wools, hence, should be applicable for other material composition than the ones listed in Table 2.1.

2.2 Uncertainty management

2.2.1 Uncertainty types

Parameter Uncertainty

In probabilistic simulations, the inputs and outputs are not single values but range represented using distributions. The parameters in a distributed sense are the parameter uncertainty.

The expression of uncertainty in output, $T = f(\mathbf{X})$, f being continuous and one time differentiable function, can be derived by Taylor expanding

T about its mean and utilizing the definition of standard deviation in T [84]. The first order approximation is,

$$\sigma_T^2 = \mathbf{J}^{\mathbf{T}} \boldsymbol{\Sigma}^{\mathbf{X}} \mathbf{J}, \tag{2.15}$$

where σ_T^2 represents variance in T, $\boldsymbol{\Sigma}^{\mathbf{X}}$ is variance-covariance matrix of the input vector, $\mathbf{X}$, and $\mathbf{J} = (J_1, J_2, J_3...)$, $J_i = \partial f / \partial X_i$. For complex and non-linear problems, derivation of Eq 2.15 is mathematically challenging, therefore, stochastic methods are adopted.

Modelling uncertainty

The modelling uncertainty is the inaccuracy of the models in perfectly reflecting the reality. It is quantified using the systematic bias, δ, and the second central moment of random errors, σ_ϵ, by comparing the simulated, $\hat{T}$, and true distribution, T [85],

$$\delta = \frac{\mu_{\hat{T}}}{\mu_T}, \quad \text{and} \quad \sigma_\epsilon = \left[\frac{1}{N-1} \sum_{i=1}^{N} \left(\hat{T}_i - \delta \cdot T_i \right)^2 \right]^{\frac{1}{2}}, \tag{2.16}$$

where $\hat{T}_i$ and T_i are the i^{th} realization of the simulated and the true quantity respectively and N is the sample size.

Sampling Uncertainty

The dependence of probabilistic outputs upon the sample size and sampling method is sampling uncertainty. Figure 2.5 illustrates such uncertainty. The simulated distribution $\hat{T}$, correct distribution, T, and the 95 percent fractiles values, z_{95}, are presented for sample sizes N=100, 1000 and 10000. Higher sample size well represents the distribution.

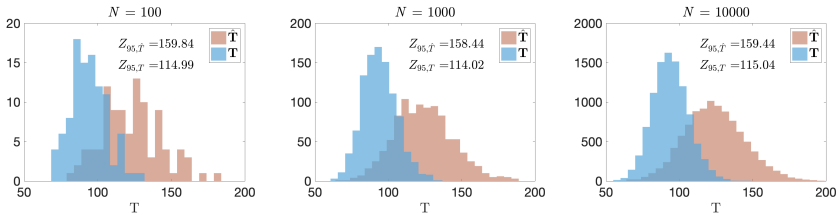

Figure 2.5. The distributions of simulated values, $\hat{T}$, true values, T, and 95 percent fractiles for three different sample sizes N=100, 1000 and 10000.

2.2.2 Combining model and parameter uncertainty

The output for a simulation model, $T = f(X)$, with systematic bias, δ, and random error, ϵ, is

$$\hat{T} = \delta \cdot T + \epsilon, \tag{2.17}$$

where $\hat{T}$ is the simulated quantity and T is the true quantity. Here, the T and ϵ are independent and the mean of ϵ is zero. For such conditions, the mean and variance of the observed quantity can be written as [86],

$$\mu_{\hat{T}} = \delta \cdot \mu_T \quad \text{and} \quad \sigma^2_{\hat{T}} = \delta^2 \cdot \sigma^2_T + \sigma^2_\epsilon, \tag{2.18}$$

where μ_T and σ^2_T are the mean and variance of the true quantity and σ^2_ϵ is the variance of the random error.

2.2.3 Eliminating model uncertainty

If the prior information of δ and σ_ϵ is available, one can correct the simulated output towards the true one. The expression of corrected output is [86]

$$T = \frac{1}{\delta}\left[\mu_{\hat{T}} + \left(\hat{T} - \mu_{\hat{T}}\right)\sqrt{1 - \left(\frac{\sigma_\epsilon}{\sigma_{\hat{T}}}\right)^2}\right], \tag{2.19}$$

where T is the corrected realization corresponding to the observed realization, $\hat{T}$.

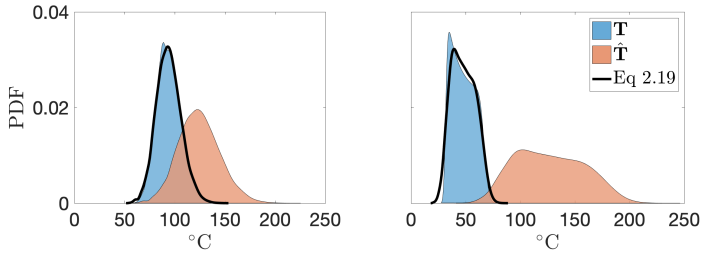

Figure 2.6. Upper: The true, T, simulated, $\hat{T}$, and corrected distributions.

I illustrate the correction method using two arbitrarily chosen examples [87]. One example using Gaussian shape, and another example using an irregular shape. First, I calculate the correction parameters, 2.16. Then I used the parameters to obtain the true shape from the simulated one.

Figure 2.6 shows the true, simulated and corrected distributions, which indicate that the corrected distribution matches well with the true distribution.

2.2.4 Quantifying sampling uncertainty

The sampling uncertainty can be quantified as $\pm$ bounds from the corrected value [82]. For example, if the probability inferred from the corrected distribution is p, then the probability is $p \pm \Delta p$, where Δp is the sampling uncertainty. In LHS, sampling uncertainty estimation needs the convergence analysis. Figure 2.7 shows the result of the convergence analysis carried out for the distributions presented in Figure 2.5. The corrected z_{95} and the sampling uncertainty with N = 1000, are 61 and 2 respectively. Thus, the 95 per cent fractiles value is 61$\pm$2.

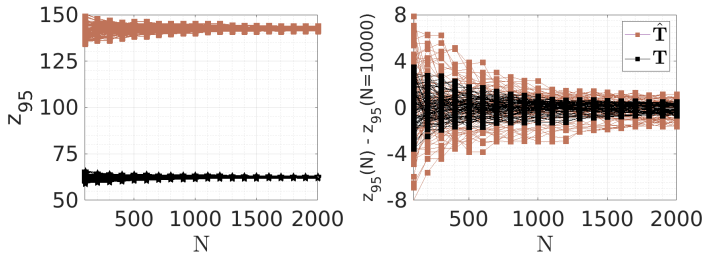

Figure 2.7. Left: The 95 percent fractiles value, z_{95}, of the simulated, $\hat{T}$, and corrected, T, distributions for different sample size, N. Right: The difference of $z_{95}(N)$ and the converged value, $z_{95}(N = 10000)$.

2.3 Probabilistic simulation

2.3.1 Monte Carlo (MC) analysis

The chosen method for sampling and probabilistic simulation is LHS and MC, respectively. For LHS, I divide the cumulative density function (CDF) of each variable into N partitions. Then I randomly choose one value from each partition and obtain a list of N values for each variable. Then I select one value from each list and form an input sample. I then repeat it N times and get N input samples.

LHS produces converged solutions with comparatively small sample size,

hence is a computationally cost-effective method for the MC simulations [78, 79]. For fire barrier resistance evaluations, the distribution shapes of input uncertainties are not well established. Therefore, I mostly use Normal or Uniform shapes that are popular in risk analysis.

2.3.2 Meta-models

Response Surface Model

The common approach in RSM is to express inputs, $\mathbf{X} = x_1, x_2, ..., x_n$, and output, $\hat{T}(\mathbf{X})$, using quadratic (second order) polynomial function,

$$\hat{T}(\mathbf{X}) = a + \sum_{i=1}^{n} b_i x_i + \sum_{i=1}^{n} c_i x_i^2 + \sum_{i=1}^{n-1} \sum_{j=i+1}^{n} d_{ij} x_i x_j, \tag{2.20}$$

and to estimate the coefficients, a, b_i, c_i, d_{ij}, by satisfying Eq.2.20 with known design points.

I present a generic expression suitable for an arbitrary order, m, and arbitrary number of input parameters, n,

$$\widehat{T}(\mathbf{X}, t) = \sum_{i=1}^{M} a_{i,t} \prod_{j=1}^{n} x_j^{\mathbf{Mn}_{ij}}, \qquad M = \frac{\prod_{i=1+m}^{n+m} i}{\prod_{i=1}^{n} i}, \tag{2.21}$$

where, t represents time, $a_{i,t}, i = 1, 2, ..., M$, are the coefficients and $\mathbf{Mn}_{M\times n}$ is a multinomial matrix containing the powers terms of the polynomials obtained using Algorithm 1, See Appendix.

For $n = 2$ and $m = 2$, the multinomial matrix and the response surface would be,

$$\mathbf{Mn}_{M\times n} = \begin{bmatrix} 0 & 0 \\ 0 & 1 \\ 0 & 2 \\ 1 & 0 \\ 1 & 1 \\ 2 & 0 \end{bmatrix}, \quad M = \frac{4\times 3}{2\times 1} = 6 \quad \text{and,}$$

$$\begin{aligned} \widehat{T}(x_1, x_2, t) &= a_{1,t} x_1^0 x_2^0 + a_{2,t} x_1^0 x_2^1 + a_{3,t} x_1^0 x_2^2 + a_{4,t} x_1^1 x_2^0 + a_{5,t} x_1^1 x_2^1 + a_{6,t} x_1^2 x_2^0 \\ &= a_{1,t} + a_{2,t} x_2 + a_{3,t} x_2^2 + a_{4,t} x_1 + a_{5,t} x_1 x_2 + a_{6,t} x_1^2. \end{aligned} \tag{2.22}$$

At each time instance, the RSM coefficients are assumed to be independent of other time instances, and therefore separately estimated.

Gaussian Processes Model

In GP Regression, the prediction is based on the GP of mean, $m(\mathbf{x})$, and the covariance, $k(\mathbf{x}, \mathbf{x}')$, of the collected functions, $f(\mathbf{x})$, that are consistent to the known inputs, $\mathbf{x} = [\mathbf{x}^1, ..., \mathbf{x}^M]$, and outputs, $\mathbf{f} = [f(\mathbf{x}^1), ..., f(\mathbf{x}^M)] = [\mathbf{y}^1, ..., \mathbf{y}^M]$,

$$\begin{aligned} m(\mathbf{x}) &= \mathbf{E}\left[f(\mathbf{x})\right], \\ k(\mathbf{x}, \mathbf{x}') &= \mathbf{E}\left[(f(\mathbf{x}) - m(\mathbf{x}))(f(\mathbf{x}') - m(\mathbf{x}'))^{\mathbf{T}}\right], \\ f(\mathbf{x}) &\sim \mathcal{GP}\left(m(\mathbf{x}), k(\mathbf{x}, \mathbf{x}')\right) \end{aligned} \tag{2.23}$$

where $f(\mathbf{x})$ and $f(\mathbf{x}')$ are jointly Gaussian, and k is positive definite also known as the kernel function [62, 61, 63].

The most commonly used kernels are Linear(Ln), Rational Quadratic(RQ) and Square Exponential(SE) also known as Gaussian or radial basis function. Ln is the product of inputs, $k_{\text{Ln}}(\mathbf{x}_1, \mathbf{x}_2) = \mathbf{x}_1 \cdot \mathbf{x}_2$. RQ is the mixture of many SE functions [63],

$$k_{\text{RQ}}(\mathbf{x}_1, \mathbf{x}_2) = \alpha \left(1 + \exp\frac{||\mathbf{x}_1 - \mathbf{x}_2||^2}{\beta 2l^2}\right)^{-\beta}, \tag{2.24}$$

where α and l are the variance and the length scale. The RQ becomes identical to SE when the power term, $\beta \to \infty$. The kernel is selected in such a way that its shape is close to the deterministic solution that I aim to approximate.

Including the unknown outputs, $\mathbf{f}_* = [f(\mathbf{x}_*^1), ..., f(\mathbf{x}_*^M)]$, corresponding to $\mathbf{x}_* = [\mathbf{x}_*^1, ..., \mathbf{x}_*^M]$, the Gaussian process, i.e., Eq 2.23, takes the form,

$$\begin{bmatrix} \mathbf{f} \\ \mathbf{f}_* \end{bmatrix} \sim \mathcal{N}\left(\begin{Bmatrix} m(\mathbf{x}) \\ m(\mathbf{x}_*) \end{Bmatrix}, \begin{bmatrix} K_{ff} & K_{f_*f}^{\mathbf{T}} \\ K_{f_*f} & K_{f_*f_*} \end{bmatrix}\right), \tag{2.25}$$

where $K_{f_*f} = K(X_*, X)$ denotes $M \times M$ matrix of covariances evaluated at all pairs of known and unknown points, and similarly for K_{ff} and $K_{f_*f_*}$. The posterior distribution is then the joint distribution of the functions

that is consistent with the known inputs and outputs,

$$P(\mathbf{f}_*|\mathbf{f}) \sim \mathcal{N}\left(K_{f_*f}K_{ff}^{-1}\mathbf{f}, \quad K_{f_*f_*} - K_{f_*f}K_{ff}^{-1}K_{f_*f}\right). \tag{2.26}$$

For the time-dependent problem, a single deterministic case can be extrapolated as several study cases. For this, the time points need to be stacked as an additional input vector. For example, with n input parameters, M data points, and Nt time points, the input and output can be stacked as,

$$\mathbf{x} = \begin{bmatrix} \mathbf{x}^1 \\ \mathbf{x}^2 \\ \mathbf{x}^3 \\ \vdots \\ \mathbf{x}^M \end{bmatrix}, \ \mathbf{x}^i = \begin{bmatrix} x_1^i & x_2^i & x_3^i & \cdots & x_n^i & t_1 \\ x_1^i & x_2^i & x_3^i & \cdots & x_n^i & t_2 \\ x_1^i & x_2^i & x_3^i & \cdots & x_n^i & t_3 \\ \vdots & \vdots & \vdots & \vdots & \vdots & \\ x_1^i & x_2^i & x_3^i & ... & x_n^i & t_{Nt} \end{bmatrix}, \ \mathbf{f} = \begin{Bmatrix} \mathbf{y}^1 \\ \mathbf{y}^2 \\ \mathbf{y}^3 \\ \vdots \\ \mathbf{y}^M \end{Bmatrix}, \ \mathbf{y}^i = \begin{Bmatrix} y_1^i \\ y_2^i \\ y_3^i \\ \vdots \\ y_{Nt}^i \end{Bmatrix},$$

where $t_1, t_2, \cdots, t_{Nt}$ represent times and $i = 1, 2, \cdots, M$ represent data points. The number of study points are now $M \times Nt$.

2.3.3 Application: Stone wool thermal resistance

I estimate stone wool layer cold side temperature for a range of time-temperature curves depicting various compartment fire scenarios [88]. Figure 2.8 shows the time-temperature curves, the location of the stone

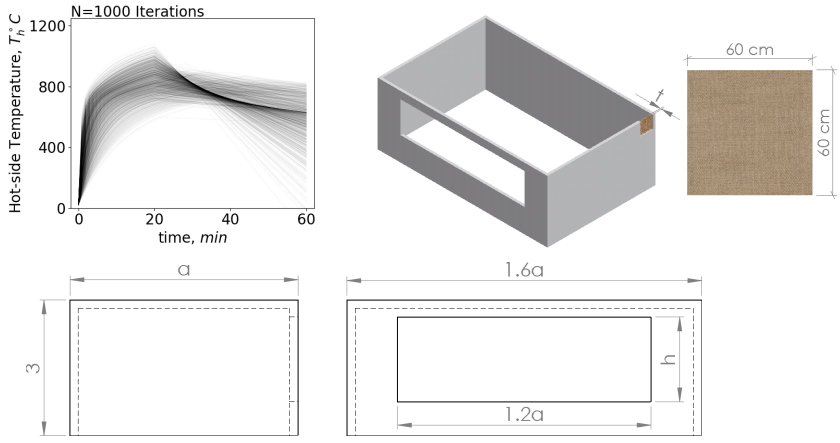

Figure 2.8. Upper left: A parametric time-temperature curve representing various compartment fire scenarios. Upper right: Location of the stone wool protective layer. Lower: A fire compartment with enclosure size: $1.6a \times a \times 3.0$ m^3 and opening size: $1.2a \times h$ m^2.

wool layer, and the geometry of the compartment. The floor and ceiling are concrete, and the walls are Gypsum board. Table 2.3 lists the material properties. The curves represent office building compartment fire

Table 2.3. Material properties and thickness of the compartment boundaries.

Item	Material	Thickness l(m)	Density ρ (kgm^{-3})	Specific heat c_p(Jkg^{-1}K^{-1})
Walls	Gypsum board	0.12	710	1050
Ceiling/Floor	Concrete	0.3	2280	1040

according to Annex A of EN 1991-1-2:2000.

The random inputs are the width, a, height of the opening, h, fire load density, $q_{\mathrm{f,t}}$, the thermal diffusivity of walls, α_{w}, and the thermal diffusivity of ceiling or floor, α_{f}. The samples size is N=1000, and the sampling method is LHS. Table 2.4 lists their mean and standard deviation or the lower and upper values.

Table 2.4. The input parameter distributions for the fire scenarios.

Input parameters	Distribution	Mean	Standard deviation	Lower	Upper	Unit
Room width, a	Uniform	-	-	3	7	m
Opening height, h	Uniform	-	-	1	2	m
Fire load density, $q_{\mathrm{f,d}}$	Uniform	-	-	200	700	MJm^{-2}
Ceiling/Floor thermal diffusivity, α_{f}	Normal	1E-6	1E-7	-	-	m^{2}s^{-1}
Wall thermal diffusivity, α_{w}	Normal	7.6E-7	7.6E-8	-	-	m^{2}s^{-1}

Figure 2.9 shows the steps of stochastic simulation. For the first $2M$=100 sampling points, I carried out deterministic FEM simulations. Using the deterministic points, I constructed the meta-models and quantified the meta-modelling uncertainty. Then I carried out the remaining MC iterations using the meta-model, and finally, corrected the predicted realizations using Eq 2.19.

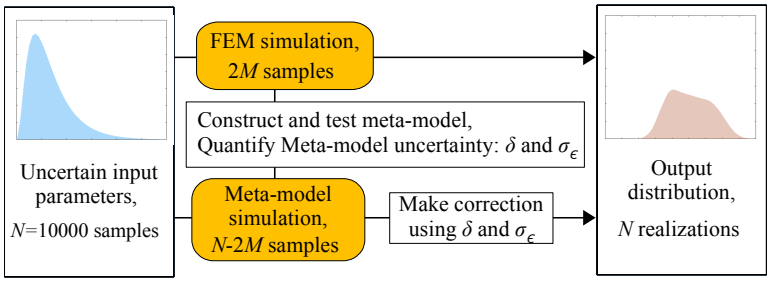

Figure 2.9. Schematic diagram showing the steps of the stochastic analysis.

I studied three wool types (7, 22 and 30) listed in Tables 2.1. The selected wools property differs notably from one another: the amount of organic content is low in wool 7, and the wools differ from one another in terms of density.

3. Results

3.1 Stone wool thermal resistance

3.1.1 Validation

Cold-side temperatures

The fire resistance tests were simulated and the cold-side temperatures were predicted using both multiphysics and heat conduction model. Fig-

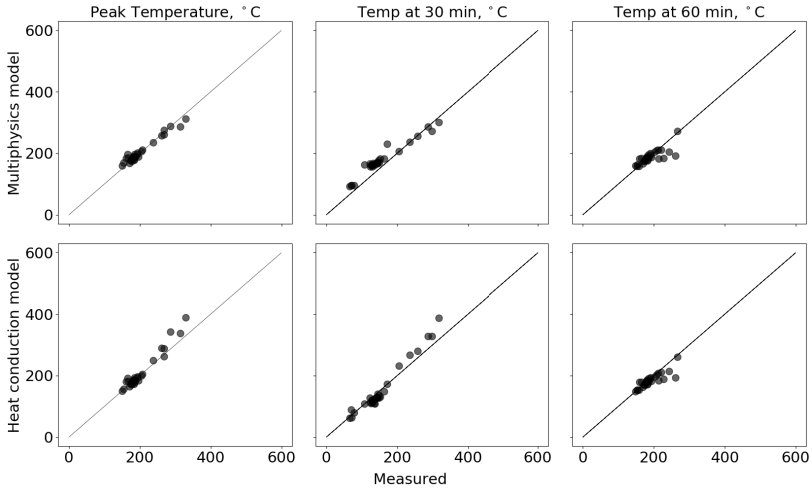

Figure 3.1. The scatter plots of the measured and predicted cold-side temperatures.

ure 3.1 shows the scatter plots of the peak values and the temperatures at 30 and 60 minutes obtained from all the tests. The scatter values are aligned along the diagonal, and the models have similar performance for

the prediction of the temperature at a specific time. The peak temperatures predicted by the multiphysics model are comparatively close to the diagonal, and this is because of accurate modelling of the release of the reaction heat.

Time to critical temperatures

To evaluate the models' capability to predict fire resistance times, the times of the cold side rising above an arbitrary critical temperature T_{Cr} were determined from the time-temperature curves. Figure 3.2 shows

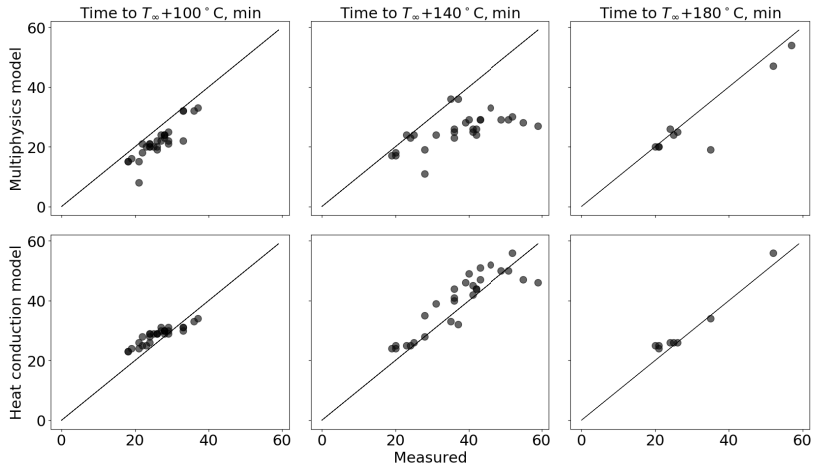

Figure 3.2. The scatter plots of the times at which the cold-side rises by 100, 140 and 180 °C.

the scatter plots of the times at which the cold side temperature rises by 100, 140 and 180 °C. The plots show that the values for the heat conduction and multiphysics models are slightly above and below the diagonal, respectively. The heat conduction model predictions are closer to the diagonal. It is interesting to note here that the time predictions are more accurate with the heat conduction model despite its poor performance for the prediction of the peak temperature.

Modelling Uncertainty

Figure 3.3 shows the modelling uncertainty, $\delta \pm \widetilde{\sigma}_\epsilon$, for temperature and time predictions, calculated using the scatter values presented in Figure 3.1 and 3.2 respectively. N=30 for all the listed outputs except "time to $T_\infty + 140°$C" and "time to $T_\infty + 180°$C". For these quantities, N=28 and N=8 respectively, see Figure 3.2. The last two are the average values of the out-

puts. The plot indicates that the multiphysics model over-predicts tem-

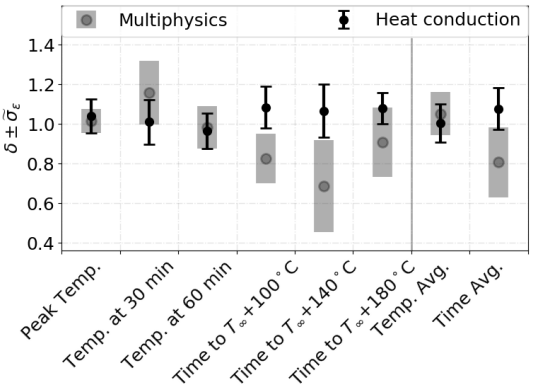

Figure 3.3. Modelling uncertainty, $\delta \pm \widetilde{\sigma}_\epsilon$, in temperature and time prediction.

peratures and under-predicts times, whereas the heat conduction model over-predicts times. In average, the temperature predictions between the model is negligibly biased, while the time predictions are notably biased.

3.1.2 Qualitative analysis

Using the multiphysics model, the field variables (temperature, organic mass %, and oxygen availability) were estimated along the thickness of the stone wools. The plots in Figure 3.4 show the profiles of these quantities for wools 7, 22 and 30, at times 10, 20 and 40 min. The temperature plots (first row) show how the cold side temperatures start to grow after 10 min. At 20 min, the cold side temperature gradients of the wools 7 and 22 become similar to the hot side gradients and exceed the hot size gradients for wool 30. Low- density -wools have a higher thermal conductivity at high temperatures than the high-density wool, and thus the exothermic heat is transferred easier.

The second row shows the organic matter mass concentration. The plots indicate that the oxidative degradation propagates from the hotter-side to the colder-side. For wool 22, some portion of the organic matter remains unreacted on the hotter side because there is no oxygen available (lower middle plot) for oxidative decomposition, due to the high generation of product gas (high organic content sample). For wools 7 and 30, the organic matter decomposition is uninterrupted. Some degree of oxygen limitation is observed in these wools as well (lower, left and right plot) but that does

not last for long because the product gas generation is low (low organic content sample).

The third row shows the oxygen availability. The y-axis value 1 means that the porous media is fully air, and 0 means that the air is not available. The plots indicate that for the wool 7 (left plot), the product gas never covers the entire porous region, i.e., the oxygen is always available. The time-wise change in the curves is most significant for wool 30 (middle and right plots). This means the faster air recovery for a wool with comparatively smaller organic mass %.

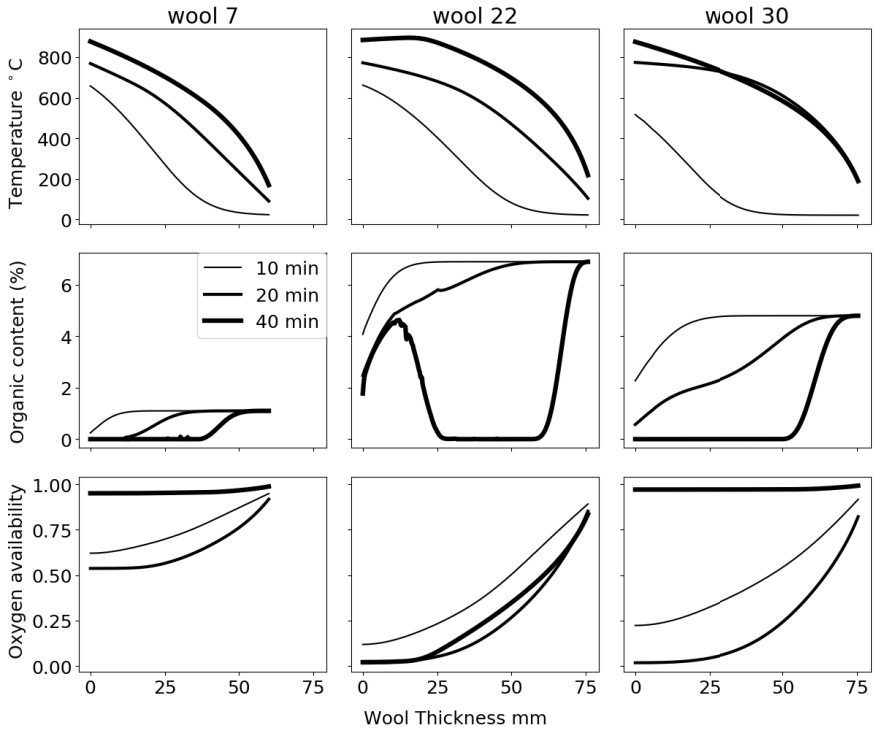

Figure 3.4. Temperatures, organic content mass %, and oxygen availability along with the thickness of wool 7, 22 and 30, and at 10, 20 and 40 minutes.

3.1.3 Sensitivity to mass transfer

I estimated the cold-side temperatures for a different ratio of gas diffusion and heat transfer coefficient. The plots in Figure 3.5 show the results for $\frac{D_2}{h_2} = 2\mathrm{E}-4, 6\mathrm{E}-4, ..., 1.8\mathrm{E}-3$, which indicate that the curve peak decreases with an increase in the gas diffusion, for wool 22 and 30. Thus, for the high organic content stone wool, the high fire resistivity

(low-temperature peak) can be achieved by reducing the gas transfer.

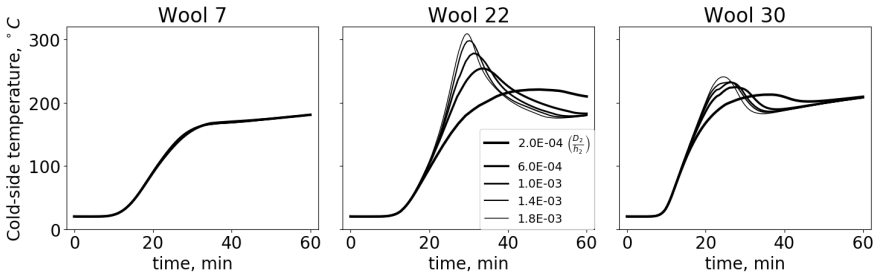

Figure 3.5. Cold-side temperature sensitivity to the ratio of gas diffusion and heat transfer coefficient, $\frac{D_2}{h_2}$.

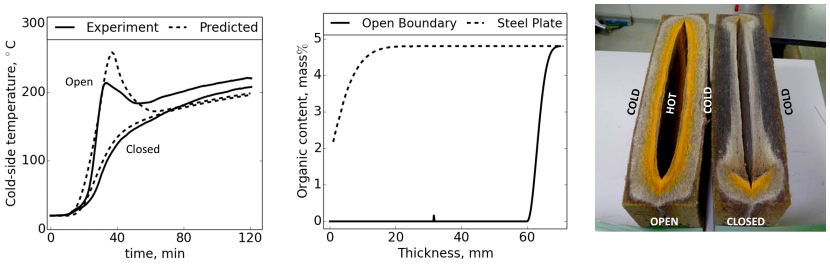

Figure 3.6. Sensitivity to open or closed boundary. Left: Cold-side temperatures. Middle: Organic mass % at the end of test. Right: Visual inspection of the decomposition zone at the end of test.

The significance of the oxygen transfer on temperature histories was further confirmed by carrying out two additional experiments with stone wool containing 4.8% organic matter. In the first test, the steel plate was placed only on the hot side, as before. In the second test, steel plates were placed on both sides. The measured and predicted (multiphysics model) cold side temperatures are shown in the left plot of Figure 3.6. The temperature peak is not observed for the wool with closed boundaries. In both cases, the predicted temperatures are mostly in good agreement with the measured temperatures. However, after the exothermic peak in the open-boundary case, the nearly steady-state temperature is slightly under-predicted by the model. The middle plot in Figure 3.6 shows the predicted organic content at the end of the tests. It indicates that for the open boundary wool, the decomposition occurs throughout the thickness, but reaches only up to $\sim$ 20 mm for the closed one. This prediction resembles the decomposition zone seen in the photograph of the samples taken after dissecting them into half. The photograph shows also that the thick-

ness of the open boundary -wool (left sample) has decreased more than that of the closed one (right sample).

3.2 Uncertainty quantification and compensation

3.2.1 Concrete wall thermal resistance

I tested the uncertainty quantification and compensation method for concrete wall temperature estimation, using the predicted and measured data of a compartment fire experiment [89]. The experiment consisted of 20 tests, varying in fire size, location, and opening door width, see Table 3.1. The predictions were using FDS [10].

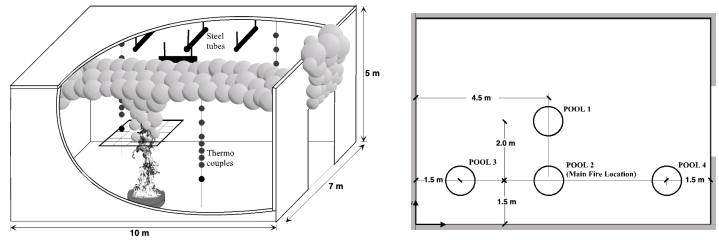

Figure 3.7. Left: Schematic diagram representing the fire experiment. Right: The selected pool locations.

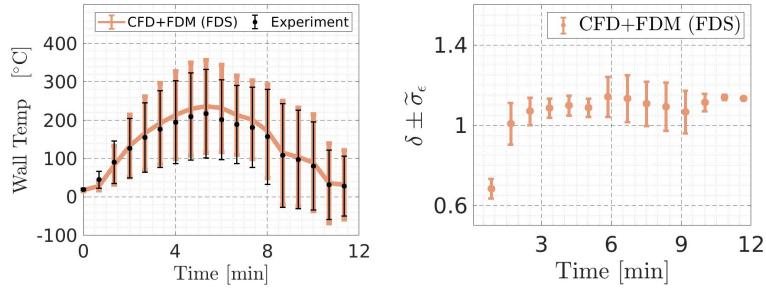

Figure 3.8. Left: The two moments of the predicted and measured wall temperature. Right: Model uncertainty, $\delta \pm \sigma_\epsilon$.

The left plot in Figure 3.8 compares the measured and the predicted wall temperature in terms of their first two moments. The right plot visualizes the model uncertainty, $\delta \pm \widetilde{\sigma}_\epsilon$, at each time. The plots show that the measured and the predicted values are close to each other. In average,

Table 3.1. Fire test series: Fire size, fire location and opening door width.

Test No.	Pool location	Pool diameter(m)	Pool Area (m^2)	Duration (min)	Door width(m)
Test 0	2	0.71	0.4	4:00	2.4
Test 1	2	0.71	0.4	4:00	2.4
Test 2	2	0.71	0.4	8:27	2.4
Test 3	2	0.88	0.6	7:45	2.4
Test 4	2	0.88	0.6	7:55	2.4
Test 5	2	0.88	0.6	8:14	2.4
Test 6	3	0.88	0.6	7:55	2.4
Test 7	1	0.88	0.6	8:00	2.4
Test 8	1	0.88	0.6	7:45	2.4
Test 9	4	0.88	0.6	7:18	2.4
Test 11	2	1.17	1.0	5:15	2.4
Test 12	2	1.17	1.0	5:07	2.4
Test 13	2	1.17	1.0	5:21	2.4
Test 15	1	1.17	1.0	5:15	2.4
Test 16	1	1.17	1.0	5:20	1.2
Test 17	2	1.17	1.0	5:20	1.2
Test 18	2	1.17	1.0	5:29	1.2
Test 19	2	1.60	2.0	5:30	2.4
Test 20	2	1.60	2.0	9:30	2.4

the wall temperatures are slightly over predicted. Most importantly, I see that the model uncertainties at different time instances are not identical.

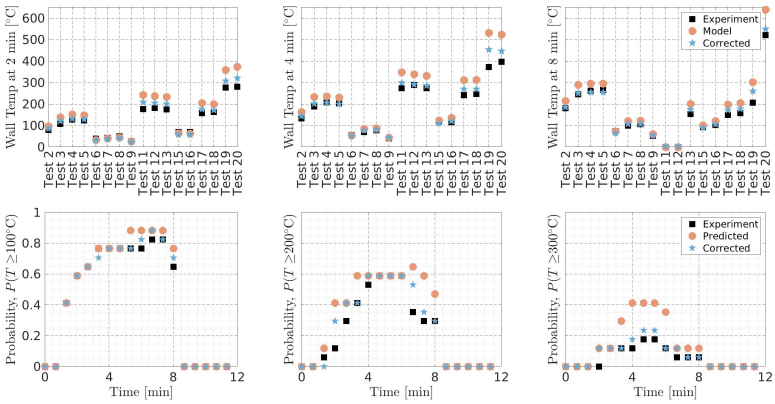

Figure 3.9. Upper: The predicted, measured and corrected wall temperatures. Lower: Probability that the wall crosses a given threshold in a given time.

The upper plots in Figure 3.9 shows the predicted, measured and the corrected wall temperatures at different times for each of the tests. The temperatures were corrected using the average values of model uncertainty parameters ($\delta = 1.15$, $\widetilde{\sigma}_\epsilon = 0.16$). The plots show that the prediction and measurement are apart, and the corrected value is usually closer to the measurement. The lower plots show the failure probabilities at differ-

ent times for different threshold temperatures. The predicted probabilities are higher than the measured ones, and the corrected probability values are closer to the measured ones. The results indicate that the model uncertainty values can be generalized for the correction of temperature and failure probability. Here the uncertainty parameters are from the same validation campaign used for the testing of the method. In the validation guides, however, the uncertainty parameters are calculated from the result of numerous fire experiment, hence represent more generalized values.

3.2.2 Stone wool thermal resistance

I tested the uncertainty compensation for the stochastic simulation scenario of predicting stone wool cold side temperature. The simulation scenario is the same as the one presented in section 2.3.3 with slight modification in the random inputs, see Table 3.2, where I add a new variable, i.e., Wool type, to select a type of stone wool material from 30 different varieties listed in Table 2.1.

Table 3.2. The input parameter distributions for the fire scenarios.

Input parameters	Distribution	Mean	Standard deviation	Lower	Upper	Unit
Room width, a	Uniform	-	-	2	7	m
Opening height, h	Uniform	-	-	1	2.4	m
Fire load density, $q_{\mathrm{f,d}}$	Uniform	-	-	200	900	MJm^{-2}
Wall thermal diffusivity, α_{w}	Normal	1E-6	1E-7	-	-	$\mathrm{m}^2\mathrm{s}^{-1}$
Ceiling/Floor thermal diffusivity, α_{f}	Normal	7.6E-7	7.6E-8	-	-	$\mathrm{m}^2\mathrm{s}^{-1}$
Wool type	Discrete	-	-	1	30	

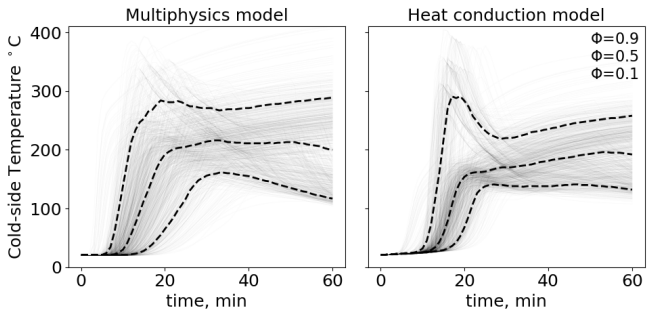

Figure 3.10. The cold-side temperature solution space obtained from the stochastic analysis. The dotted curves represent ϕ=0.1, 0.5 and 0.9 fractile value of the distribution.

Figure 3.10 shows the predicted cold-side temperature solution space.

The dotted line represents the Φ=0.1, 0.5 and 0.9 fractile value of the distribution. The plots indicate that the bell-shaped region, in the case of the multiphysics model, covers a relatively wide time range($\sim$ 10 to $\sim$ 40 min). With the heat conduction model, the oxidative reactions start later, but after the initiation, the reactions take place faster, covering a narrower range of time ending by $\sim$30 min.

Figure 3.11 compares the Cumulative Density Functions (CDF) for peak temperature, temperatures at 30 and 60 min, and times for three different threshold temperatures corresponding to the temperature increase by 100, 140 and 180°C. The time CDF curves for the 140 and 180 degree temperature increase end below unity because these threshold temperatures were reached in only a fraction of the simulated fires. These distributions were calculated by first collecting the statistics of the cases where the criterion was met, and then normalizing the curve with the share of those cases. The plots show that there can be large discrepancies in the time distributions despite the small discrepancy in the peak temperature distributions. For most output quantities, the differences between model distributions comply with the test uncertainty metrics in Figure 3.3. The only exception is "Time to $T_\infty + 180$°C", for which, the discrepancy in the distribution is larger than the discrepancy in the biases shown in Figure 3.3. The reason is probably related to the small size of the data behind the validation metrics.

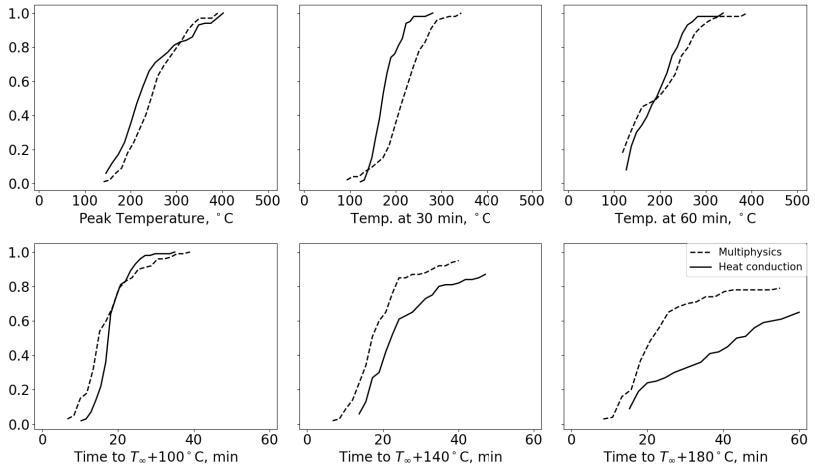

Figure 3.11. The cumulative density functions for temperature and time prediction. The dotted and continuous line respectively represent the multiphysics and heat conduction models.

Next, I apply the uncertainty compensation model, Eq. 2.19, and the average value of δ and $\widetilde{\sigma}_\epsilon$, Figure 3.3, to calculate the corrected outputs. After correcting all values, the new distributions were created (Figure 3.12). Based on the visual evaluation, I can say that the best improvement is seen in $T_\infty + 140°$C. The results indicate that the uncertainty compensation is most effective for the outputs which are quantitatively but not qualitatively different, and for which the difference of the predicted statistics complies with the validation metrics (Figure 3.3).

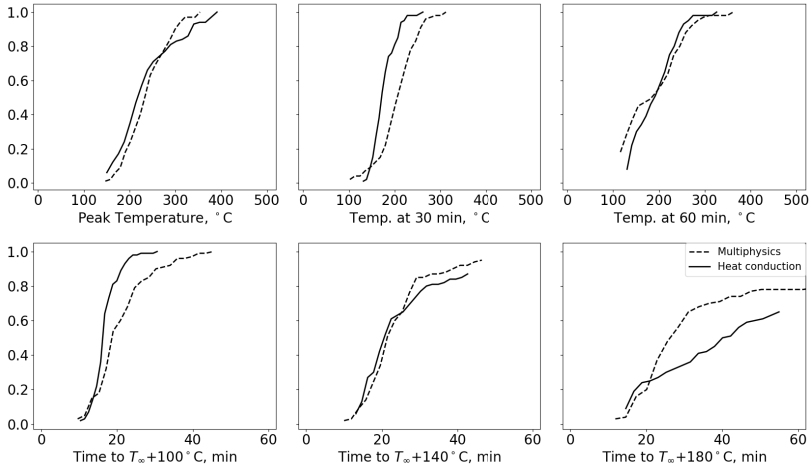

Figure 3.12. The corrected cumulative density functions for temperature and time prediction. The dotted and continuous line respectively represent the multiphysics and heat conduction models.

3.2.3 A chain of two models

I investigated the uncertainty propagation for a modelling scenario involving two numerical models in a chain: The gas model output T_h serves as an input to the wall model from which I observe the output as the cold-side temperature, $T_2 = f_\mathrm{W}(T_\mathrm{h}, \alpha)$, where f_W is a conduction model solving the heat diffusion equation for the vector of material properties, α, listed in Table 3.3.

For this, I carry out MC analysis of f_w, for three different types of boundary condition and six different types of distributions of the gas model output T_h and the wall model inputs α. Table 3.3 lists the input range and Table 3.4 lists the study cases. The model, $T_2 = f_\mathrm{W}(T_\mathrm{h}, \alpha)$, was assumed to be an ideal model that produces an error-free output. Model errors were

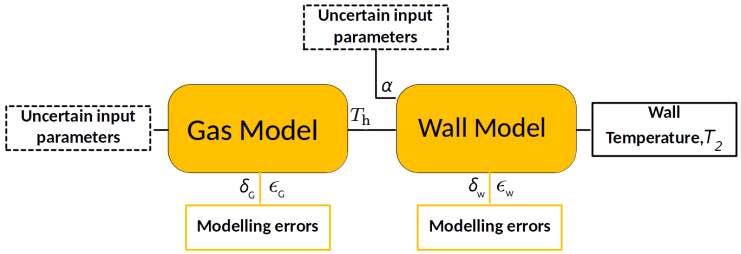

Figure 3.13. The modeling chain.

then imposed on T_{h} and T_2 as bias and random error. For both models, the relative bias factor was $\delta = 1.1$ and the random errors were sampled from a normal distribution with a relative second central moment $\widetilde{\sigma}_\epsilon \equiv \sigma_\epsilon/\mu = 0.1$.

Table 3.3. Parameters of the distributions presenting stochastic uncertainties.

Input parameters	Mean,μ	Standard deviation, σ	Lower value	Upper value	Unit
Gas Temperature,T_{h}	1200	100	780	1580	$[^{\circ}C]$
Thermal conductivity, k	1	0.1	0.6	1.4	$[Wm^{-1}K^{-1}]$
Specific Heat Capacity, c_{p}	2200	200	1400	2900	$[JKg^{-1}K^{-1}]$
Density, ρ	900	90	530	1260	$[Kgm^{-3}]$
Heat transfer coefficient, h	9	0.7	6	12	$[Wm^{-2}k^{-1}]$
Emissivity, e	0.7	0.07	0.4	1	$[Wm^{-2}k^{-1}]$

Table 3.4. Study cases.

S.N.	Symbol	Heat-flux	Gas temperature	Wall parameters
1	conv.u.s	convective	uniform	single
2	conv.u.u	convective	uniform	uniform
3	conv.u.n	convective	uniform	normal
4	conv.n.s	convective	normal	single
5	conv.n.u	convective	normal	uniform
6	conv.n.n	convective	normal	normal
7	rad.u.s	radiative	uniform	single
8	rad.u.u	radiative	uniform	uniform
9	rad.u.n	radiative	uniform	normal
10	rad.n.s	radiative	normal	single
11	rad.n.u	radiative	normal	uniform
12	rad.n.n	radiative	normal	normal
13	both.u.s	both	uniform	single
14	both.u.u	both	uniform	uniform
15	both.u.n	both	uniform	normal
16	both.n.s	both	normal	single
17	both.n.u	both	normal	uniform
18	both.n.n	both	normal	normal

After the MC simulation, I calculate the propagated modelling-errors by

comparing the error-free and the simulated distributions. The propagated modelling-errors (left plot, Figure 3.14) indicate that the error propagation is independent of the type of input parameter distribution. They are, however, sensitive to the type of heat flux. In case of the convective heat flux, the propagated bias $\delta\{\mathrm{G,W}\}$ is simply a product of individual biases, but with radiation, the bias values are lower, as the nonlinear heat loss compensates for the increased surface temperature.

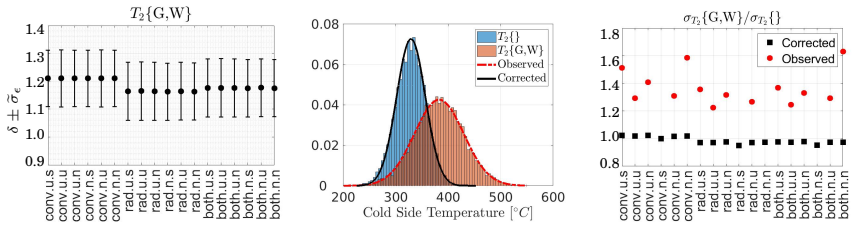

Figure 3.14. Left: The propagated model-error in cold-side surface temperature estimation. Middle: An example estimation of the error-free distribution from the simulated one. Right: Observed and corrected standard deviation normalized by the error-free value.

The middle plot shows an example of the observed, error-free, and the corrected distribution. The plot indicates that the corrected distribution match to the error-free distribution. The right plot shows the observed and corrected standard deviations normalized by the error-free value. The ratio improves from above 1.2 to nearly 1 in all study cases. The results indicate that the uncertainty compensation method is applicable also for a chain of numerical models, and it requires the quantified information of the propagated model errors.

3.3 Meta-model based stochastic simulation

3.3.1 Validation

As a proof of concept to meta-model based stochastic simulation and uncertainty correction, I carry out MC simulation (Figure 3.15), compare the stochastic performance of actual FEM model and the meta-model, and test if error compensation method indeed reduces the discrepancy between two different types of predictions. I do this using a simple example of the thermal resistance evaluation (Section 2.1.2) of Gypsum wall pre-

sented in Figure 2.8. The MC simulation, $N = 1000$, is using both FEM and the meta-models, and the meta-model training and testing are using $2M$ number of FEM realizations. Figure 3.16 compares the temperatures corresponding to the instantaneous cumulative distribution function values Φ=0.1,0.5 and 0.9. The plots show that, in general, the meta-model predictions are in good agreement with the FEM model except the 1st and 3rd order RSM, which deviate from FEM results in the early/late stage of the fire. Best results are obtained with 2nd order RSM and GP model having highest number of training points, $M = 50$.

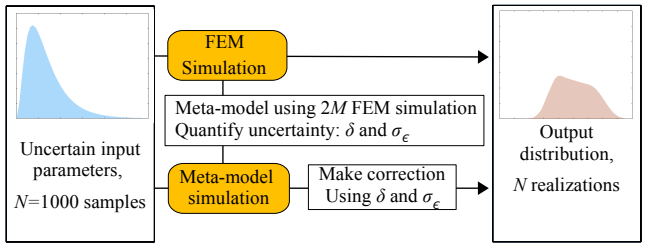

Figure 3.15. Steps for meta-model based stochastic analysis, a proof of concept.

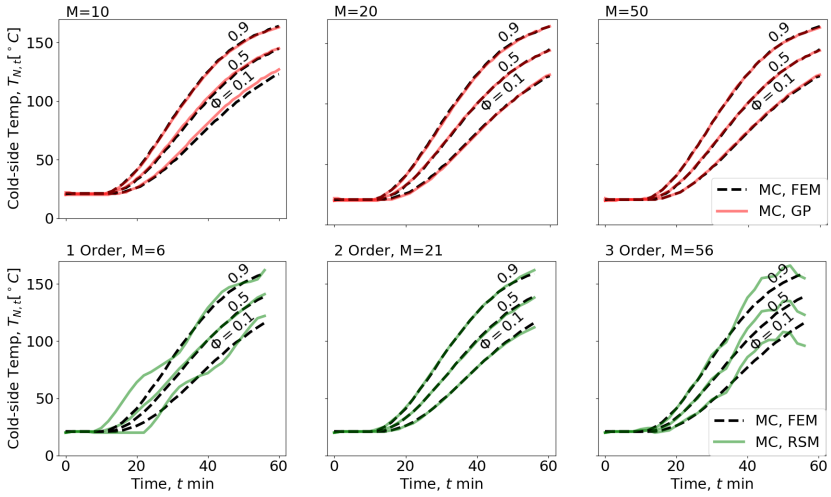

Figure 3.16. Comparison of cold-side temperatures in terms of 10, 50 and 90% fractiles values of the predicted distributions. Upper plots: GP vs FEM. Lower plots: RSM vs FEM.

Figure 3.17 compares the probability of rising above $T_\infty + 140 = 160°$C, obtained using four different methods of computation. The data labelled

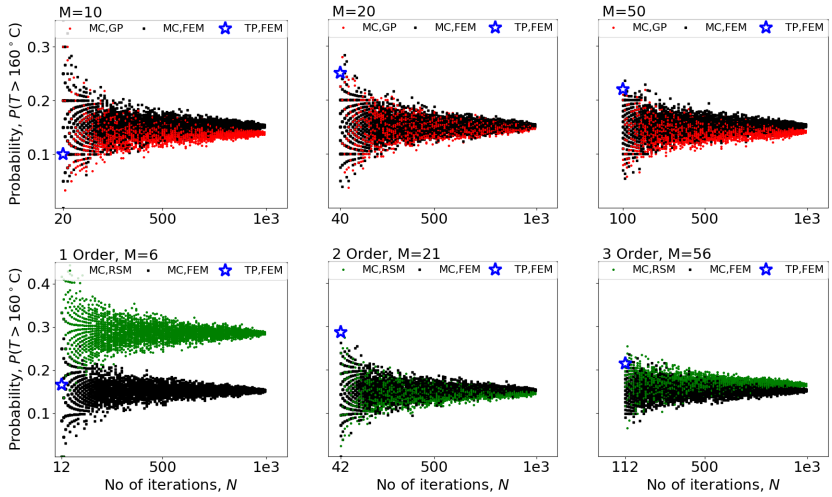

Figure 3.17. Convergence plot for the probability that the cold-side temperature rise above $160°$C. Upper: FEM vs GP model. Lower: RSM vs FEM.

'MC, FEM', 'MC, GP', and 'MC, RSM' correspond to the stochastic results with FEM and the GP and RSM surrogate models, respectively. The number of MC iterations, N, was varied between a case-dependent minimum and 1e3. The 'TP, FEM' represents the probability value calculated using the deterministic training and test points, i.e., the fraction of training and test cases crossing the threshold in reference to the total number of training and test cases. The plots indicate that the probabilities obtained from the MC simulations converge when N increases close to 1e3. With $N = 100$, the uncertainty of the probability estimates is about 30 %. Overall, the converged probabilities from the meta-model MC are close to that of FEM except for the 1^{st} order RSM. Interestingly, the probabilities corresponding to the 3^{rd} order RSM, which performed poorly in the accuracy tests above, are only slightly above the correct values. This is because the peak-temperature probability density functions match exactly at $160°$C. The GP model with M=20 provides the most accurate estimate of the probabilities. The results show that both the RSM or GP models can be useful in improving the probability estimation.

Next, I take a closer look at two meta-models that performed poorly in the above analysis. Figure 3.18 left and middle plot show the cold-side temperatures that, at each time point, correspond to the value $\Phi = 0.05$ of the cumulative density function, i.e. 5% fractile, of the GP model

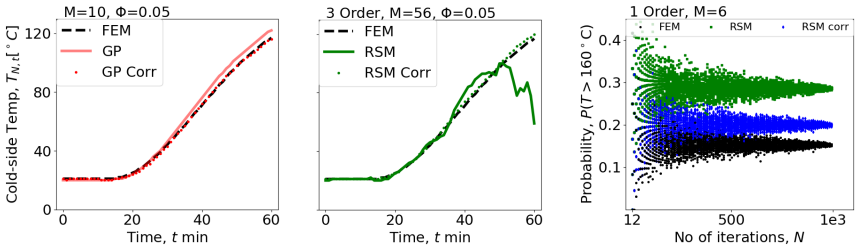

Figure 3.18. Comparison of the predicted and corrected outputs. Left and Middle Plot: The cold-side temperatures with cumulative density, $\Phi = 0.05$. Right Plot: The probability of crossing the threshold temperature.

with M=10 and 3$^{\text{rd}}$ order RSM. Both GP and RSM results are successfully corrected towards the FEM result, although the correction is much more drastic for the 3$^{\text{rd}}$ order RSM. The right plot shows the uncorrected and corrected probabilities of exceeding the threshold temperature for the 1$^{\text{st}}$ order RSM. Corrected probabilities are closer to the FEM probabilities, but a significant ($\approx$ 25 %) over-prediction in probability remains.

3.3.2 Application: Stone wool thermal resistance

Next, I carry out the meta-model based MC simulation presented in Section 2.3.3. Figure 3.19 compares the 10 %, 50% and 90 % ($\Phi = 0.1, 0.5$ and 0.9) fractiles of the cold-side temperature distributions from the test points, calculated with FEM and GP ($M = 50$). Qualitatively, the tem-

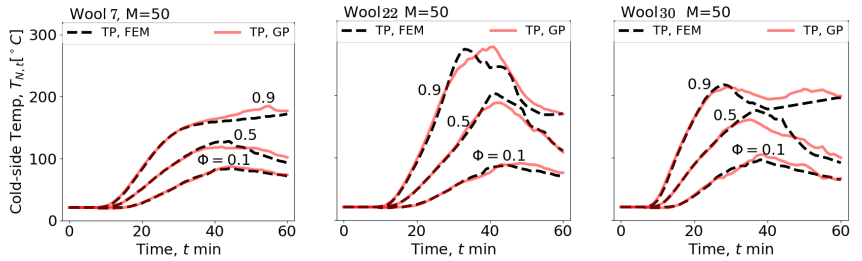

Figure 3.19. Testing of the GP model: Meta-model prediction vs deterministic FEM realization.

peratures behind Wool 7 are low and the exothermic peaks are not visible. This is due to high density, which slows down the heat transfer, and low organic content, which leads to low exothermic heating. The highest temperatures are obtained for Wool 22, due to its high organic content. The plots indicate that the GP meta-model predicts accurately the rising phase of the temperature but not falling. Fortunately, this is sufficient

for the reliability estimation because the probability of crossing a threshold temperature depends only on how the temperature rises to the peak value.

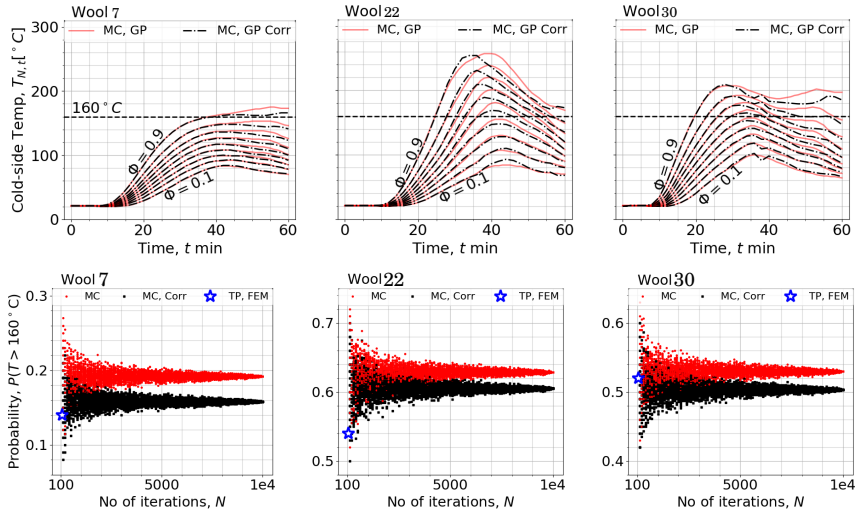

Figure 3.20. Upper: The cold-side temperatures corresponding to the cumulative density, Φ=0.1,..,0.9. Lower: The probability that the cold-side temperature rises above $T_\infty + 140 = 160°\text{C}$.

Figure 3.20 shows the distributions of the cold-side temperatures in terms of cumulative density, Φ, for uncorrected and corrected GP results. The black dashed lines represent the threshold temperature, $T_\infty + 140 = 160°\text{C}$, for which the probabilities are shown in the lower plots. The red and black colored dots represent the probabilities calculated using the predicted and corrected MC realizations, respectively. The blue star-shaped marker represents the probability calculated using FEM at the training points. The plot indicates that the probability estimated using N=100 (sum of test and training points) would be somewhere between 0.05 and 0.3 for Wool 7, 0.4 and 0.8 for Wool 22 and 0.4 and 0.7 for Wool 30. Using the metamodel I can achieve converged, predicted or corrected probabilities, which would be 0.16 and 0.195 for Wool 7, 0.605 and 0.63 for Wool 22, and, 0.505 and 0.53 for Wool 30.

4. Discussion

The modelling uncertainties of heat conduction and multiphysics models show that the stone wool temperature predictions are less uncertain with the heat conduction model. The results defy the general understanding that the inclusion of a higher number of mechanisms improves the prediction. They comply with the findings of Bal and Rein [90], that, sometimes, mechanism simplification improves model predictions. In this study, however, solving more mechanism helps in explaining the effect of the porous media oxygen transfer on the overall heating behaviour of stone wools. Additionally, including more mechanisms improves model sensitivity to the change in material properties and boundary conditions [82]. In real applications, the choice of modelling method also depends on the computational costs, and in this regards, simple pyrolysis model can be more time-efficient than solving the entire porous media mass transfer physics.

The factor that determines the oxygen unavailability in the stone wool is the amount of organic matter. Livkiss et al. [29] observed that ignoring the dependency of degradation reactions on the oxygen availability leads to inaccurate temperature estimation for high density and high organic content stone wools. They concluded that the low porosity is the cause of the oxygen unavailability in the high-density stone wools. Considering the stone wools studied in this work the porosity is high ($\geq$0.95) regardless of the stone wool density (38 to 147 kg·m^{-3}). The high density, thus, does not necessarily affect the oxygen transfer. One example is Wool 7 (100 kg·m^{-1}), for which the temperature profiles are unchanged for different values of gas diffusion coefficients, see Figure 3.6. The confusion arises because the amount of organic matter may be the same despite the difference in either density or LOI. For example, the amount of organic

matter in 100 kg·m^{-3} stone wool with 5% LOI is same as in 50 k·gm^{-3} wool with 10% LOI. It seems that the lack of oxygen transfer is seen either in the samples with high LOI or the high-density samples with sufficient LOI. In the current study, the lack of oxygen transfer occurred for the stone wools with organic content above 2.3 kg·m^{-3}.

The study tests the uncertainty quantification and compensation method using four different modelling scenarios: in Section 3.2.1 for the concrete wall temperature in 20 different fire tests using the uncertainty metric of the same validation set; in Section 3.2.3 for the outputs of a chain of numerical models using the uncertainty metrics obtained from the MC simulation of the same chain of models; in Section 3.2.2 for the temperature estimation of a randomly chosen stone wool material subjected to an uncertain fire condition using the uncertainty metrics of separate validation tests consisting of a single fire condition and in Section 3.3.1 for the meta-model stochastic prediction using the uncertainty metrics of meta-model training and test data. The method proved to be effective in all the cases except the one in section 2.3.3, where the correction parameters (Figure 3.3) do not fully match with the discrepancies in the stochastic outputs (Figure 3.16). In other words, the validation cases are not generic enough. The stone wool properties (Table 2.1) do not vary systematically, and the fire conditions are limited to only ISO 834 standard fire. For a highly non-linear problem as the heat transfer of porous, reactive material with many dependent variables (organic mass %, density, thickness, fibre orientation, intact fibre %), the 30 validation tests were too few for the generalization the model uncertainty.

The provision for the simulation-based fire barrier resistance evaluation would be that the prediction uncertainties are systematically quantified, which requires the management of different types of uncertainties resulting from the using of the simulation tools. The study in Figure 4.1 presents the overall procedure for uncertainty management. The modelling uncertainty is quantified in terms of δ and $\widetilde{\sigma}_\epsilon$, and the outputs are corrected using the quantified parameters and Eq 2.19. The δ and $\widetilde{\sigma}_\epsilon$ can be from the studied validation campaign or from the validation guides consisting of several similar validation campaigns [46]. The quantification of sampling uncertainty is performed using the convergence analysis of the distribution moments, as illustrated in Section 2.2.1. Unlike the

modelling uncertainty, the sampling uncertainty is not compensated but is quantified as $\pm$ bound of the predicted output.

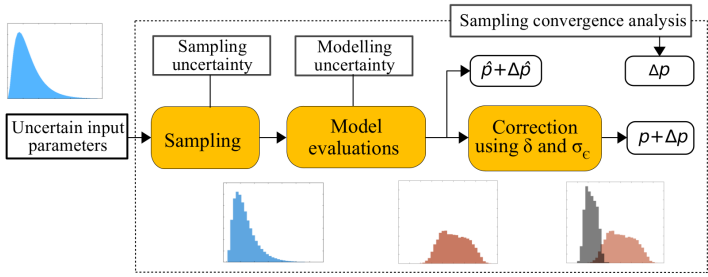

Figure 4.1. Schematic diagram showing the procedure of uncertainty management in stochastic simulations.

For a time consuming thermal resistance model or when the fire load condition needs expensive numerical methods such as Computational Fluid Dynamics (CFD), the MC simulation can be performed using the meta-models. Figure 4.2 shows the overall procedure of uncertainty management for such cases. The first step is to obtain the training and test points using the deterministic simulations. Then the next step is to correct the training and test points using the known uncertainty metrics, δ_1 and $\sigma_{\epsilon 1}$. The meta-model construction is using the corrected deterministic points. The meta-modelling uncertainty metrics, δ_2 and $\sigma_{\epsilon 2}$, are quantified during the testing of the meta-models. Finally, the MC simulation is carried out using the meta-models, and the predicted realizations are corrected using δ_2 and $\sigma_{\epsilon 2}$. The sampling convergence analysis is performed using both corrected and uncorrected meta-model realizations.

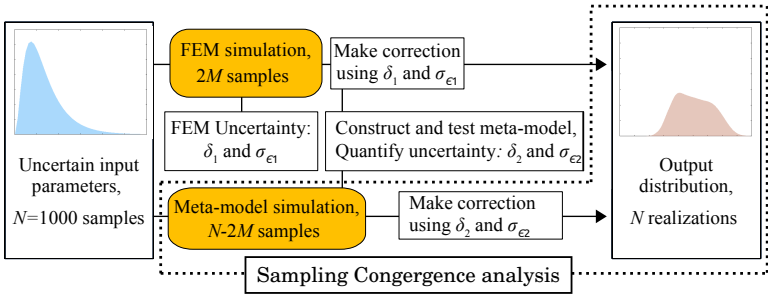

Figure 4.2. Schematic diagram showing the procedure of uncertainty management in the meta-model based stochastic analysis.

The scheme presented in Figure 4.2 uses a stochastic process for the full

probabilistic distribution, meta-modelling to reduce the computational cost, and the uncertainty model to compensate for the model uncertainties. It is thus useful to study the robustness of conservative methods such as the Design of Experiments (DOE), BEPU, and analytical solutions that are generally inaccurate for the local optima, and in which the model uncertainty management is not justifiable due to the lack of full distributed solutions.

The presented approach, in addition to uncertainty estimation, can be used for product optimization, which helps in reducing the number of tests required for product certification. Also, such an approach can certify the products whose properties, compared to that of the tested ones, vary under the limit specified in the European standard for extended application, EN 15254-3:2019. For example, the thickness can vary by up to 50%. The possible hurdles for such simulation-based certification, however, are the lack of detailed information on barrier material properties, demanding user skills for schemes presented in Figure 4.1, or 4.2, and lack of test data for the generalization of validation metrics.

From the viewpoint of risk analysis applications, the procedures, shown in Figures 4.1 and 4.2, should be implemented into a simulation platform, where the steps exempt to user routine-work are automatically solved in the background. The existing examples of such simulation platforms are the Probabilistic Fire Simulator (PFS) [91] and AAMKS [92], where the deterministic simulations, the sampling methods, and the supercomputing setups automatically run in the background. Sometimes, however, the problem scenario may not perfectly fit in the structure of such dedicated platforms, and the choice is up to the user whether to implement custom versions for Figure 4.1 or 4.2, or entirely new simulation platform.

Although I present this model to support fire barrier resistance evaluation, it can be applied in other studies where there is a need for uncertainty management, and more effectively in the analysis scenario where the model uncertainty adequately propagates to the output distribution. Regarding the distribution shape representing the uncertainty, I also illustrate this method using an example of irregular distribution (Section 2.2.3). The application, therefore, does not have to be limited to only Normal or Uniform type of distribution.

5. Conclusions

In this thesis, I studied the challenges of the simulation-based evaluation of fire barrier thermal resistance. The challenges are the numerical modelling of heating inside fibrous layer, the high computational cost due to the input uncertainty-originated requirement of large-scale stochastic simulations, and the propagation of model uncertainty to the stochastically simulated output uncertainty. For the simulation of heating inside fibrous barriers, I presented a multiphysics approach of modelling stone wool heating, and alternative heat conduction -based approach coupled to the LOI-dependent reaction kinetics. The capability of the models to predict the cold-side temperature of different stone wools was studied by validating against experimental data and by sensitivity and stochastic analyses.

The multiphysics model shows that the stone wool temperature depends upon the availability of oxygen. In the stone wools with high organic content, the oxygen entrainment, the oxidative degradation and the exothermic release of heat are suspended due to the high rate of product gas production. Both types of models were found to be capable of reproducing experimentally observed bell-shaped, exothermic peaks in the case of high organic content -stone wools and continuous temperature profiles otherwise, with $\pm 20\%$ uncertainty. The good performance of the multiphysics model was a consequence of including the essential physical phenomena, but for the heat conduction model, the good performance required kinetic coefficients to be correlated with LOI is possibly limiting its generality.

The models predict the expected response to variation in material composition and hot-side boundary conditions. Considering the use of unshielded and sandwich-type stone wool products in fire protection, I ob-

served that the peak cold-side temperature of the high organic content -stone wool could be effectively reduced by preventing the flow on the cold side. A thin layer of non-permeable material, thus, can be used to block oxygen transfer and to increase the fire resistivity of high organic content stone wools.

As an alternative to the high computational cost of the probabilistic simulation, I investigated the use of RSM and GP meta-models. The results show that both RSM and GP meta-models enable us to achieve converged stochastic predictions of the output distributions and failure probabilities, even with the limited number of deterministic data points. The simple polynomial based RSM was found to fail when the heat-transfer was affected by exothermic reactions of the stone wool. Fortunately, this is in contrast with GP, where the kernel combination made the approximation possible even for such a case.

For the uncertainty management, I formulated a simple method of distinguishing the model uncertainty from the stochastically simulated output distribution. I then illustrated it in different analysis scenarios: concrete wall thermal resistance, stone wool thermal resistance, a chain of two models, and meta-modelling. The results show that the method effectively corrects the simulated output towards more accurate value when the uncertainty correction metric well represents the model uncertainty of the investigated analysis scenario. The modelling uncertainties reported in the context of the model validation, thus, can be used for correcting the output distributions resulting from parameter (input) uncertainty.

The findings serve as a proof of concept for the simulation-based reliability analysis of fire barriers and hence substantially support the communication between the fire safety community and the authorities. In particular, it supports the performance-based fire barrier design regulation, the implementation of which has been limited due to the lack of clarity of the roles of probabilistic analysis and uncertainty management methods.

6. Future work

The modelling accuracy for the stone wool thermal resistance can be further improved. The current models assume the stone-wool to be a continuum domain and solve the problem using the equivalent definition of the thermal properties. The alternative methods for the accurate modelling of the thermal properties have not been explored. Also, the porous media mass transfer is solved using only the mass diffusion physics. One may consider further development of the model including the momentum conservation and the Darcy laws as illustrated by Weber [93] for the Gypsum board. Additionally, to accurately predict the final cold side temperature, I had to prescribe the reduction of the stone wool thickness. The thickness shrinkage is likely due to the high-temperature lead structural deformation of the fibres. Future modelling efforts may consider the fibre mechanical response to a high temperature, to improve temperature predictions.

The modelling is also limited to completely dry samples of stone wool. In real-life applications, however, the insulating properties are also affected by humidity [94]. The long term material exposure to ambient increases the structure moisture content and alter the thermal conductivity [95]. Additionally, the moisture also weakens the mechanical strength of fibres and alter the overall load-bearing capacity of the structure. For the wider application of modelling, future studies may consider humidity for both insulating property and load-bearing capacity.

In regards to uncertainty correction, the proposed method is effective with fully complying correction parameters. For stone wool temperature prediction, the modelling uncertainty metric needs generalization. This requires new tests with systematically varied fire conditions and material

properties.

On the cost-effective stochastic analysis methods, the current study limits its scope to two (RSM and GP) of the popular methods. One may test the performance of other alternatives such as Neural Network (NN), Bayesian optimization technique, Markov Chain Monte Carlo (MCMC).

Appendix: Multinomial matrix calculation

Algorithm 1 creates Multinomial Matrix, ***Mn***, which represents the power terms of Response Surface Method (RSM) model presented in Section 2.3.2.

Algorithm 1 Multinomial Matrix

$m \leftarrow$ Polynomial order
$n \leftarrow$ No of variables
M ← ((m+1)(m+2)*(m+3)..(m+n)) / (1*2*3..n)*
[**Mn**] ← M rows and n columns
$\{\mathbf{Mn}_{1..m+1,1}\} \leftarrow \{0, 1, .., m\}^T$
$\{C\} \leftarrow \{1, 2, .., m+1\}$
for `im = 2,3,...,n` **do**
    $\{S2\} \leftarrow \{C_{m+1}, C_{m+1}, ..., C_{m+1}\}_{(m+1)\times 1}$
    $\{S1\} \leftarrow C_{m+1} - \{0, C_1 - 1, C_2 - 1, .., C_m - 1\}$
    $\{C\} \leftarrow$ Cumulative Sum$\{C\}$
    $\{D2\} \leftarrow C_{m+1} - \{0, C_1, C_2, .., C_m\}$
    $\{D1\} \leftarrow \{D2_2, D2_3, .., D2_{m+1}, 1\}$
    for `in = 1,2,..,m+1` **do**
        $\left[\mathbf{Mn}_{D1_{\text{in}},..,D2_{\text{in}},\quad 3,..,\text{im}}\right] \leftarrow \left[\mathbf{Mn}_{S1_{\text{in}},..,S2_{\text{in}},\quad 2,..,\text{ip}-1}\right]$
        $\{\mathbf{Mn}_{D1_{\text{in}},..,D2_{\text{in}},\quad 2}\} \leftarrow \{\mathbf{Mn}_{S1_{\text{in}},..,S2_{\text{in}},\quad 1}\} - \{\mathbf{Mn}_{S1_{\text{in}},\quad 1}\}$
        $\{\mathbf{Mn}_{D1_{\text{in}},..,D2_{\text{in}},\quad 1}\} \leftarrow \{\mathbf{Mn}_{S1_{\text{in}},1}, \mathbf{Mn}_{S1_{\text{in}},1}, .., \mathbf{Mn}_{S1_{\text{in}},1}\}_{(D2_{in}-D1_{in}+1)\times 1}$

Bibliography

[1] Andres, B., Livkiss, K., Hidalgo, J.P., van Hees, P., Bisby, L., Johansson, N. and Bhargava, A., 2018. Response of stone wool–insulated building barriers under severe heating exposures. *Journal of fire sciences*, 36(4), pp.315-341.

[2] Yvon, P. and Carré, F., 2009. Structural materials challenges for advanced reactor systems. *Journal of Nuclear Materials*, 385(2), pp.217-222.

[3] Schroll, R.C., 2016. Industrial fire protection handbook. CRC press. 252 p.

[4] Buchanan, A.H. and Abu, A.K., 2017. Structural design for fire safety. John Wiley & Sons. 438 p.

[5] Khoury, G.A., 2000. Effect of fire on concrete and concrete structures. *Progress in Structural Engineering and Materials*, 2(4), pp.429-447.

[6] Pereira, D., Gago, A., Proença, J. and Morgado, T., 2016. Fire performance of sandwich wall assemblies. *Composites Part B: Engineering*, 93, pp.123-131.

[7] Joyeux, D., 2002. Experimental investigation of fire door behaviour during a natural fire. *Fire safety journal*, 37(6), pp.605-614.

[8] Wald, F., Chlouba, J., Uhlíř, A., Kallerova, P. and Štujberová, M., 2009. Temperatures during fire tests on structure and its prediction according to Eurocodes. *Fire safety journal*, 44(1), pp.135-146.

[9] Hadjisophocleous, G.V. and Bénichou, N., 2000. Development of performance-based codes, performance criteria and fire safety engineer-

ing methods. *International Journal on Engineering Performance-Based Fire Codes*, 2(4), pp.127-142.

[10] McGrattan, K., Hostikka, S., McDermott, R., Floyd, J., Weinschenk, C. and Overholt, K., 2013. Fire dynamics simulator technical reference guide volume 1: mathematical model. NIST special publication, 1018(1), 175 p.

[11] Lee, S.R. and Ryou, H.S., 2006. A numerical study on smoke movement in longitudinal ventilation tunnel fires for different aspect ratio. *Building and Environment*, 41(6), pp.719-725.

[12] Shen, T.S., Huang, Y.H. and Chien, S.W., 2008. Using fire dynamic simulation (FDS) to reconstruct an arson fire scene. *Building and environment*, 43(6), pp.1036-1045.

[13] Drean, V., Schillinger, R., Leborgne, H., Auguin, G. and Guillaume, E., 2018. Numerical simulation of fire exposed facades using LEPIR II testing facility. *Fire technology*, 54(4), pp.943-966.

[14] Yu, L.X., Beji, T., Maragkos, G., Liu, F., Weng, M.C. and Merci, B., 2018. Assessment of numerical simulation capabilities of the fire dynamics simulator (fds 6) for planar air curtain flows. *Fire technology*, 54(3), pp.583-612.

[15] Zadeh, S.E., Maragkos, G., Beji, T. and Merci, B., 2016. Large eddy simulations of the ceiling jet induced by the impingement of a turbulent air plume. *Fire Technology*, 52(6), pp.2093-2115.

[16] Jujuly, M.M., Rahman, A., Ahmed, S. and Khan, F., 2015. LNG pool fire simulation for domino effect analysis. *Reliability Engineering & System Safety*, 143, pp.19-29.

[17] Matala, A. and Hostikka, S., 2011. Probabilistic simulation of cable performance and water based protection in cable tunnel fires. *Nuclear Engineering and Design*, 241(12), pp.5263-5274.

[18] Hietaniemi, J., 2007. Probabilistic simulation of fire endurance of a wooden beam. *Structural Safety*, 29(4), pp.322-336.

[19] Buchanan, A.H., 1999. Implementation of performance-based fire codes. *Fire Safety Journal*, 32(4), pp.377-383.

[20] Alvarez, A., Meacham, B.J., Dembsey, N.A. and Thomas, J.R., 2013. Twenty years of performance-based fire protection design: challenges faced and a look ahead. *Journal of Fire Protection Engineering*, 23(4), pp.249-276.

[21] Zehfuss, J. and Hosser, D., 2007. A parametric natural fire model for the structural fire design of multi-storey buildings. *Fire Safety Journal*, 42(2), pp.115-126.

[22] Hadjisophocleous, G.V., Benichou, N. and Tamim, A.S., 1998. Literature review of performance-based fire codes and design environment. *Journal of Fire Protection Engineering*, 9(1), pp.12-40.

[23] Van Coile, R., Hopkin, D. and Lange, D., 2019. Guest Editorial: Probabilistic Methods in Fire Safety Engineering. *Fire Technology* 55, pp.1107–1109

[24] Anderson, A. and Ezekoye, O.A., 2018. Quantifying generalized residential fire risk using ensemble fire models with survey and physical data. *Fire technology*, 54(3), pp.715-747.

[25] Lie, T.T. and Irwin, R.J., 1995. Fire resistance of rectangular steel columns filled with bar-reinforced concrete. *Journal of structural engineering*, 121(5), pp.797-805.

[26] Lu, H., Zhao, X.L. and Han, L.H., 2011. FE modelling and fire resistance design of concrete filled double skin tubular columns. *Journal of Constructional Steel Research*, 67(11), pp.1733-1748.

[27] Daryabeigi, K., Cunnington, G.R. and Knutson, J.R., 2013. Heat transfer modeling for rigid high-temperature fibrous insulation. *Journal of Thermophysics and Heat Transfer*, 27(3), pp.414-421.

[28] Krasnovskih, M.P., Maksimovich, N.G., Vaisman, Y.I. and Ketov, A.A., 2014. Thermal stability of mineral-wool heat-insulating materials. *Russian Journal of Applied Chemistry*, 87(10), pp.1430-1434.

[29] Livkiss, K., Andres, B., Bhargava, A. and van Hees, P., 2018. Characterization of stone wool properties for fire safety engineering calculations, *Journal of Fire Sciences*, 36(3), pp.202-223.

[30] Hasofer, A., Beck, V.R. and Bennetts, I.D., 2007. Risk analysis in building fire safety engineering. Butterworth-Heinemann, Boston, 189 p.

[31] Struck C., Almeida M. G., Monteiro da Silva S., Mateus R., Lemarchand P., Petrovski A., Rabenseifer R., Wansdronk R., Wellershoff F., de Wit J, 2015. Adaptive facade systems – review of performance requirements, design approaches, use cases and market needs, Advanced Building Skins, doi:10.13140/RG.2.1.2023.8165, pp.1254-1264.

[32] Livkiss, K., Andres, B., Johansson, N. and van Hees, P., 2017. Uncertainties in modelling heat transfer in fire resistance tests: a case study of stone wool sandwich panels. *Fire and Materials*, 41(7), pp.799-807.

[33] Chapelle, L., Lyckegaard, A., Kusano, Y., Gundlach, C., Foldschack, M.R., Lybye, D. and Brøndsted, P., 2018. Determination of the fibre orientation distribution of a mineral wool network and prediction of its transverse stiffness using X-ray tomography. *Journal of materials science*, 53(9), pp.6390-6402.

[34] Andersonm M.J. and Whitcomb, P.J., 2000. Design of experiments. *Kirk-Othmer Encyclopedia of Chemical Technology*, pp. 1-22

[35] Spitz, C., Mora, L., Wurtz, E. and Jay, A., 2012. Practical application of uncertainty analysis and sensitivity analysis on an experimental house. *Energy and Buildings*, 55, pp.459-470.

[36] D'Auria, F., 2019. Best Estimate Plus Uncertainty (BEPU): Status and perspectives. *Nuclear Engineering and Design*, 352, p.110190.

[37] Suard, S., Hostikka, S., and Baccou, J., 2013. Sensitivity analysis of fire models using a fractional factorial design. *Fire safety journal*, 62, pp.115-124.

[38] Frenklach, M., Packard, A., Garcia-Donato, G., Paulo, R., and Sacks J., 2016. Comparison of statistical and deterministic frameworks of uncertainty quantification. *SIAM/ASA Journal on Uncertainty Quantification*, 4(1), pp.875-901.

[39] Ayala, P., Cantizano, A., Sánchez-Úbeda, E.F. and Gutiérrez-Montes, C.J.F.T., 2017. The use of fractional factorial design for atrium fires prediction. *Fire technology*, 53(2), pp.893-916.

[40] Malendowski, M. and Glema, A., 2017. Development and implementation of coupling method for CFD-FEM analyses of steel structures in natural fire. *Procedia Engineering*, 172, pp.692-700.

[41] Olsson, K., Anderson, J. and Lange, D., 2017. Uncertainty propagation in FE modelling of a fire resistance test using fractional factorial design based model reduction and deterministic sampling. *Fire safety journal*, 91, pp.517-523.

[42] Martin, J.D., and Simpson, T.W., 2005. Use of kriging models to approximate deterministic computer models. *AIAA Journal*, 43(4), pp.853-863.

[43] Bichon, B.J., McFarland, J.M. and Mahadevan, S., 2011. Efficient surrogate models for reliability analysis of systems with multiple failure modes. *Reliability Engineering & System Safety*, 96(10), pp.1386-1395.

[44] Dubourg, V. and Sudret, B., 2014. Meta-model-based importance sampling for reliability sensitivity analysis. *Structural Safety*, 49, pp.27-36.

[45] McGrattan, K. and Toman, B., 2011. Quantifying the predictive uncertainty of complex numerical models. *Metrologia*, 48(3), p.173.

[46] McGrattan, K., Hostikka, S., McDermott, R., Floyd, J. and Vanella., M., 2019. Fire Dynamics Simulator Technical Reference Guide, Volume 3: Validation. NIST Special Publication no. 1018-3, Washington, DC: U.S. Departament of Commerce.

[47] Liang, B. and Mahadevan, S., 2011. Error and uncertainty quantification and sensitivity analysis in mechanics computational models. *International Journal for Uncertainty Quantification*, 1(2), pp.147-161.

[48] Gernay, T., Van Coile, R., Khorasani, N.E. and Hopkin, D., 2019. Efficient uncertainty quantification method applied to structural fire engineering computations. *Engineering Structures*, 183, pp.1-17.

[49] Ren, W.X. and Chen, H.B., 2010. Finite element model updating in structural dynamics by using the response surface method. *Engineering structures*, 32(8), pp.2455-2465.

[50] Tian, D.H., Wu, X.S., Song, Z.G. and Wang, H.Y., 2016. Reverse analysis for fire pyrolysis parameters of timber buildings based on response surface method. *Procedia Engineering*, 135, pp.19-24.

[51] Cui, C., Hu, M., Weir, J.D. and Wu, T., 2016. A recommendation system for meta-modeling: A meta-learning based approach. *Expert Systems with Applications*, 46, pp.33-44.

[52] Barbillon, P., Barthélémy, C. and Samson, A., 2017. Parameter estimation of complex mixed models based on meta-model approach. *Statistics and Computing*, 27(4), pp.1111-1128.

[53] Van Weyenberge, B., Criel, P., Deckers, X., Caspeele, R. and Merci, B., 2017. Response surface modelling in quantitative risk analysis for life safety in case of fire. *Fire Safety Journal*, 91, pp.1007-1015.

[54] Meghoe, A., Loendersloot, R. and Tinga, T., 2019. Rail wear and remaining life prediction using meta-models. *International Journal of Rail Transportation*, 8(1), pp.1-26.

[55] Tharima, A.F., Rahman, M.M., Yusoff, M.Z. and Kueh, A.B.H., 2019. Multi-objective optimization of underground car park design for tenability under fire-induced smoke. *Tunnelling and Underground Space Technology*, 85, pp.220-230.

[56] Worrell, C., Luangkesorn, L., Haight, J. and Congedo, T., 2019. Machine learning of fire hazard model simulations for use in probabilistic safety assessments at nuclear power plants. *Reliability Engineering & System Safety*, 183, pp.128-142.

[57] Lee, S.C., 1989. Effect of fiber orientation on thermal radiation in fibrous media. *International journal of heat and mass transfer*, 32(2), pp.311-319.

[58] Andersen, F.M.B. and Dyrboel, S., 1998. Modelling radiative heat transfer in fibrous materials: The use of Planck mean properties com-

pared to spectral and flux-weighted properties. *Journal of Quantitative Spectroscopy and Radiative Transfer*, 60(4), pp.593-603.

[59] Veiseh, S. and Hakkaki-Fard, A., 2009. Numerical modeling of combined radiation and conduction heat transfer in mineral wool insulations. *Heat Transfer Engineering*, 30(6), pp.477-486.

[60] Karamanos, A., Papadopoulos, A. and Anastasellos, D., 2004. Heat transfer phenomena in fibrous insulating materials. In Proceedings of WSEAS/IASME international conference on heat and mass transfer. Corfu. Greece. pp.17-19.

[61] Neal, R.M., 1997. Monte Carlo implementation of Gaussian process models for Bayesian regression and classification. Technical Report No. 9702, University of Toronto, Department of Statistics and Department of Computer Science. arXiv preprint physics/9701026. 24 p.

[62] O'Hagan, A., 1978. Curve fitting and optimal design for prediction. *Journal of the Royal Statistical Society: Series B (Methodological)*, 40(1), pp.1-24.

[63] Rasmussen, C.E., 2003. Gaussian processes in machine learning. In *Summer School on Machine Learning*. Springer, Berlin, Heidelberg. pp.63-71.

[64] Rasmussen, C.E. and Nickisch, H., 2010. Gaussian processes for machine learning (GPML) toolbox. *Journal of machine learning research*, 11, pp.3011-3015.

[65] Pedregosa, F., Varoquaux, G., Gramfort, A., Michel, V., Thirion, B., Grisel, O., Blondel, M., Prettenhofer, P., Weiss, R., Dubourg, V. and Vanderplas, J., 2011. Scikit-learn: Machine learning in Python. *Journal of machine learning research*, 12, pp.2825-2830.

[66] Neumann, M., Huang, S., Marthaler, D.E. and Kersting, K., 2015. pygps: A python library for gaussian process regression and classification. *Journal of Machine Learning Research*, 16(1), pp.2611-2616.

[67] Bouhlel, M.A., Hwang, J.T., Bartoli, N., Lafage, R., Morlier, J. and Martins, J.R., 2019. A Python surrogate modeling framework with derivatives. *Advances in Engineering Software*, 135, pp.102662.

[68] Simpson, T., Mistree, F., Korte, J. and Mauery, T., 1998. Comparison of response surface and kriging models for multidisciplinary design optimization. In 7th AIAA/USAF/NASA/ISSMO Symposium on Multidisciplinary Analysis and Optimization. St. Louis, MO, U.S.A. pp.4755

[69] Gupta, S. and Manohar, C.S., 2004. An improved response surface method for the determination of failure probability and importance measures. *Structural safety*, 26(2), pp.123-139.

[70] Box, G.E. and Wilson, K.B., 1951. On the experimental attainment of optimum conditions. *Journal of the Royal Statistical Society: Series B (Methodological)*, 13(1), pp.1-38.

[71] Edwards, I.M. and Jutan, A., 1997. Optimization and control using response surface methods. *Computers & chemical engineering, 21(4)*, pp.441-453.

[72] Gavin, H.P. and Yau, S.C., 2008. High-order limit state functions in the response surface method for structural reliability analysis. *Structural safety*, 30(2), pp.162-179.

[73] Keshtegar, B. and Kisi, O., 2017. Modified response-surface method: new approach for modeling pan evaporation. *Journal of Hydrologic Engineering*, 22(10), pp.04017045.

[74] Bateman, H., 1953. Higher transcendental functions. California Institute of Technology Bateman Manuscript Project, McGraw-Hill, New York. 316 p.

[75] Zadeh, L., and Desoer, C., 1970. Linear system theory: the state space approach. Dover Publications, McGraw-Hill, New York. 660 p.

[76] Chen, W., Jin, R., and Sudjianto, A., 2004. Analytical uncertainty propagation via metamodels in simulation-based design under uncertainty. Proceedings of the 10th AIAA/ISSMO Multidisciplinary Analysis and Optimization Conference (p.4356), Albany, New York.

[77] Le Maıtre, O.P., Knio, O.M., Najm, H.N., and Ghanem, R.G., 2004. Uncertainty propagation using wiener-haar expansions. *Journal of Computational Physics*, 197(1), pp.28-57.

[78] Robert, C., and Casella, G., 2013. Monte Carlo statistical methods. Springer Science and Business Media, New York. 509 p.

[79] Stein. M., 1987. Large sample properties of simulations using latin hypercube sampling. *Technometrics*, 29(2), pp. 143-151.

[80] Rinta-Paavola, A., 2017. Numerical simulation of passive fire protection systems. M.Sc. Thesis. Aalto University, Department of Civil Engineering. Espoo. 110 p.

[81] Zienkiewicz, O.C., Taylor, R.L. and Zhu, J.Z., 2013. The finite element method: its basis and fundamentals. Butterworth Heinemann, Oxford. 752 p.

[82] Paudel, D., Rinta-Paavola, A., Mattila, HP., and Hostikka, S., 2020. Multiphysics modelling of stone wool fire resistance. *Fire Technology, https://doi.org/10.1007/s10694-020-01050-5*, pp.1-30.

[83] Poling, B.E., Prausnitz, J.M. and O'connell, J.P., 2001. The properties of gases and liquids (Vol. 5). Mcgraw-hill, New York. 559 p.

[84] Hamilton, W.C., 1964. Statistics in physical science. Ronald Press Co., New York. 230 p.

[85] McGrattan, K. and Toman, B., 2011. Quantifying the predictive uncertainty of complex numerical models. *Metrologia*, 48(3), p. 173.

[86] Paudel, D. and Hostikka, S., 2019. Propagation of Model Uncertainty in the Stochastic Simulations of a Compartment Fire. *Fire Technology*, 55(6), pp.2027-2054.

[87] Paudel, D., and Hostikka, S., 2019. Propagation of modeling uncertainty in stochastic heat-transfer simulation using a chain of deterministic models. *International Journal of Uncertainty Quantification*, 9(1), pp.1-14.

[88] Paudel, D., and Hostikka, S., 2020. Meta-model based stochastic simulation of fire barrier cold-side temperature. *Fire Safety Journal, https://doi.org/10.1016/j.firesaf.2020.103175*, pp.1-12.

[89] Hostikka S, Kokkala M, Vaari J, 2001. Experimental study of the localized room fires: NFSC2 test series. Technical Research Centre of Finland, VTT Research Notes 2104. 49 p.

[90] Bal, N. and Rein, G., 2013. Relevant model complexity for non-charring polymer pyrolysis. *Fire safety journal*, 61, pp.36-44.

[91] Hostikka, S., Keski-Rahkonen, O. and Korhonen, T., 2003. Probabilistic Fire Simulator: Theory and User's Manual for Version 1.2. VTT Technical Research Centre of Finland. 77 p.

[92] Krasuski, A. and Hostikka, S., 2020. AAMKS-Integrated cloud-based application for probabilistic fire risk assessment. *Fire and Materials*, https://doi.org/10.1002/fam.2861, pp.1-13.

[93] Weber, B., 2012. Heat transfer mechanisms and models for a gypsum board exposed to fire. *International Journal of Heat and Mass Transfer*, 55(5-6), pp.1661-1678.

[94] Vrána, T., 2007. Impact of moisture on long term performance of insulating products based on stone wool. Doctoral thesis. KTH Royal Institute of Technology, School of Architecture and the Built Environment, Stockholm, 62 p.

[95] Karamanos, A., Hadiarakou, S. and Papadopoulos, A.M., 2008. The impact of temperature and moisture on the thermal performance of stone wool. *Energy and Buildings*, 40(8), pp.1402-1411.

Aalto-DD 186/2020

ISBN 978-952-64-0135-5 (printed)
ISBN 978-952-64-0136-2 (pdf)
ISSN 1799-4934 (printed)
ISSN 1799-4942 (pdf)

Aalto University
School of Engineering
Department of Civil Engineering
www.aalto.fi

BUSINESS + ECONOMY

ART + DESIGN + ARCHITECTURE

SCIENCE + TECHNOLOGY

CROSSOVER

DOCTORAL DISSERTATIONS